Computational Studies of 5-member Ring Heterocycles as Realkylators of Aged Acetylcholinesterase

Research Thesis

Presented in Partial Fulfillment of the Requirements for graduation *with research distinction* in The College of Arts and Sciences at The Ohio State University

by

Nathan Douglas Yoshino

The Ohio State University
May 2018

Project Advisors: Dr. Ryan J. Yoder and Dr. Christopher S. Callam
Department of Chemistry and Biochemistry

Abstract

Organophosphorus compounds (OPs) are widely implemented as chemical nerve agents and pesticides. These OPs bond to and inhibit a catalytic residue, Ser-203, in the enzyme acetylcholinesterase (AChE), which is responsible for the hydrolysis of acetylcholine. After exposure to OPs, AChE is initially inhibited for a period of time followed by an aging process, wherein the inhibited Ser-203 residue dealkylates and forms a stable phosphonate anion in the active site. There are known treatments for inhibited AChE in the form of therapeutic oximes, but no treatments for aged AChE currently exist. If left untreated, acetylcholine will build up in the central nervous system. Previous research has demonstrated quinone methides (QMs) to realkylate phosphonates and other biological molecules, which makes QMs a good candidate for an aged AChE realkylator. Previous efforts have resulted in a lead compound in the form of a quinone methide precursor (QMP). This research studies the potential of new QMPs and QMP-like compounds to realkylate the stable phosphonate anion on Ser-203 in aged AChE and allow for subsequent reactivation. With computational methods, libraries 5-member ring QMP-like compounds were tested to determine their affinity for the aged AChE active site as potential realkylators. Molecular Docking with subsequent Molecular Dynamics were used to determine compounds that favored the aged AChE active site and to elucidate the important interactions between the proposed realkylators and AChE. It was determined that substituted pyrrole based realkylators demonstrate a higher affinity for the aged active site that previously studies compounds and show promise as potential realkylators. Leaving group and charge state trends were also studied.

Acknowledgements

I must thank Dr. Christopher Callam for seeing something in me and giving me my first exposure to research. Your knowledge, and support have been invaluable to my journey and provided me the necessary foundation to move forward in my career. I especially appreciate your encouragement to follow my own ambitions and passions in research.

This brings me to my current mentor, Dr. Ryan Yoder. Thank you for inspiring an excitement of computational chemistry in me, which ultimately has set me on the course for the rest of my professional career. Your guidance and continual support will always be treasured, and I thank you the growth that I have been able to attain under you.

Of course, Dr. Christopher Hadad must be thanked for his support and overall direction of the project. I appreciate your valuable feedback and the counsel towards my future.

While not directly involved with the project, I must thank Dr. Rick Spinney, who has a substantial impact on my growth in computational chemistry. I gained so much from your classes and am grateful for the countless times you have gone above and beyond for us.

Where would we be without friends to hold us up? Rachel and Ian, I have immensely enjoyed the laughs and memories we've shared the past years which undoubtedly helped all of us through the thick. Thank you for your insights and collaboration through this project.

Perhaps most importantly, I owe most of my opportunities to my parents, Doug and Karen Yoshino, as well as my sister, Kate Yoshino. Your love and support truly has been unending and I would not be the chemist or person that I am today without you. Thank you.

Unfortunately, not everyone can be mentioned, but thank you to anyone that I have had the pleasure to interact with at my time at Ohio State. Ad Dei glorium.

List of Figures

Figure 1.1: Example of OPs used as chemical weapons and the less potent pesticide, paraxon 1
Figure 1.2: The hydrolysis of ACh via the catalytic traid (Glu-His-Ser) of AChE 2
Figure 1.3: The inhibition of the catalytic Ser-203 by phosphonylation of the OP 3
Figure 1.4: The inhibition and aging of AChE. 3
Figure 1.5: A QMP realkylating an amino acid through a QM intermediate. 4
Figure 1.6: he inhibition and aging of AChE, realkylation, and reactivation 5
Figure 1.7: RD-o-5 and derivatives that have successfully demonstrated realkylation 5
Figure 2.1: Library 1, five-member ring QMP's with varying heteroatoms 7
Figure 2.2: The respective keto-tautomers of Library 1 11
Figure 2.3: The distribution of the distance of each ligand to the aged serine residue 13
Figure 2.4: Most stable conformations of N5M and N5H 14
Figure 2.5: RD-o-5 π-stacking with Trp-86 15
Figure 2.6: N5M in the active site of aged AChE 18
Figure 2.7: O5M in the active site of aged AChE 18
Figure 2.8: RD-o-5 simultaneously hydrogen bonding with Ser-203 and Glu-202 19
Figure 3.1: Library 2, the protonated R and S keto tautomers of Library 1 21
Figures 3.2 - 3.5: The global minima enol tautomers of Library 1 23
Figure 3.6: The global minimum keto form of N5H shows ease of hydrogen bonding 24
Figure 3.7: Conformation 2, the most stable conformation without hydrogen bonding 24
Figure 3.8: BC-PO distance distribution of N5H and its keto tautomers 26
Figure 3.9: BC-PO distance distribution of N5M and its keto tautomers 26
Figure 3.10: BC-PO distance distribution of O5H and its keto tautomers 27
Figure 3.11: BC-PO distance distribution of S5H and its keto tautomers 27
Figure 3.12: N5H in the active site with VDW contacts 28
Figure 3.13: N5HR in the active site with VDW contacts 28
Figure 3.14: VDW contacts of N5MR within the aged AChE active site. 29

Figure 3.15: The distance from Gly-121 alpha carbon to the ring centroid of the ligand measurement near the oxyanion hole loop 31
Figure 3.16: O5HR nestled between the omega loop and oxyanion hole loop 31
Figure 3.17: Tyr-337 hydrogen bonding to the carbonyl group of N5MR while the ring is nestled between the omega loop and the oxyanion hole loop 33
Figure 3.18: Representative pose of OH5R in the active site during MD simulations 35
Figure 3.19: Representative pose of OH5S in the active site during MD simulations 35
Figure 4.1: Library 3, the neutral analogs of Library 1 37
Figure 4.2: Library 4, the neutral analogs of Library 2 37
Figure 4.3: BC-PO distance distribution of neutral N5H variants 39
Figure 4.4: BC-PO distance distribution of neutral N5M variants 39
Figure 4.5: BC-PO distance distribution of neutral O5H variants 40
Figure 4.6: BC-PO distance distribution of neutral S5H variants 40
Figure 4.7: The lowest energy docked conformation of Library 3 in aged AChE 41
Figure 4.8: The centroid of the Asp-74 and Trp-86 alpha carbons 43
Figure 4.9: The centroid of the Asp-74 and Trp-86 alpha carbons 43
Figure 4.10: The omega loop and Trp-86 closed in on the active site. 45
Figure 5.1: Library 5, N5H variants with different leaving groups 46
Figure 5.2: Benzylic carbon–phosphonate distance distribution for Library 5 47
Figure 5.3: The pyrrolidine sterically hindering cation-π interaction 48
Figure 5.4: N5Hdea positioned nead Trp-86 48
Figure 5.5: N5Hdea hydrogen bonding with Glu-202 across from phosphonate 50

List of Tables

Table 2.1: The relative stabilities of Library 4 and their respective tautomers (solvated) 11
Table 2.2: The relative stabilities of Library 1 and their respective tautomers (gas phase) 12
Table 2.3: Defined zones of AChE 13
Table 2.4: Percent of poses ligands spends in each region of aged AChE 14
Table 2.5: Dstribution of benzylic carbon displacement from phosphonate over time. 16
Table 2.6: Percent of time ligand hydrogen bonds to key residues 16
Table 2.7: Aromatic interactions with Trp-86 17
Table 2.8: Percent time benzylic carbon is within 4 Å of the aged residue 18
Table 3.1: The gas and solvent phase stabilities of the keto and enol tautomers 22
Table 3.2: Potential hydrogen bond measurements of enol tautomers 22
Table 3.3: Hydrogen bond measurements of keto tautomers 23
Table 3.4: Energetic favorability of intramolecular hydrogen bonding 25
Table 3.5: Lowest binding energy conformations in each frame 29
Table 3.6: Percent time benzylic carbon is within 4 Å of the phosphonate oxygen 30
Table 3.7: Percent time ligand ring centroid interacts with different structure 31
Table 3.8: Percent of time ligand acts as hydrogen bond acceptor to tyrosine residues 33
Table 3.9: Percent time ammonium hydrogen bonds or has cation-π interaction 34
Table 4.1: The relative energy of the neutral tautomers 38
Table 4.2: Percent of poses ligands spends in each region of aged AChE 40
Table 4.3: Percent time benzylic carbon is within 4 Å of the phosphonate oxygen 42
Table 4.4: Percent of time hydroxyl group acts as a hydrogen bond donor 43
Table 4.5: Measurements of the ligands structures' interactions with omega loop 44
Table 4.6: Aromatic and VDW interactions with the ring structures 45
Table 5.1: Percent of time each ligand spends in cutoff ranges from the phosphonate 48
Table 5.2: Percent of time each ligand interactions with Trp-86 49
Table 5.3: Percent of time each ligand hydrogen bonds to the phosphonate 49

Table of Contents

Abstract i
Acknowledgements ii
List of Figures iii
List of Tables v
Table of Contents vi
1. Introduction 1
    1.1 Organophosphorus Comopunds and Acetylcholinesterase 1
    1.2 Quinone Methide Presursors as Potential Realkylating Agents 4
    1.3 References 6
2. Library 1: Protonated 5-member Ring Heterocycles 7
    2.1 Introduction 7
    2.2 Methodology 8
    2.3 Enol Stability and Tautomerization 11
    2.4 Molecular Docking Results 13
    2.5 Molecular Dynamics Results 16
    2.6 References 20
3. Library 2: Protonated Keto Tautomers 21
    3.1 Introduction 21
    3.2 Stability and Conformation 22
    3.3 Molecular Docking Results 26
    3.4 Molecular Dynamics Results 30
4. Libraries 3 & 4: Neutral Variants 37
    4.1 Introduction 37
    4.2 Molecular Docking Results 39
    4.3 Molecular Dynamics Results 42
5. Library 5: Varied Leaving Group 46
    5.1 Introduction 46
    5.2 Molecular Docking Results 47

5.3 Molecular Dynamics Results 48
5.4 References 51
6. Conclusions and Future Work 52
6.1 Conclusions 52
6.2 Future Work 54

1. Introduction

1.1 Organophosphorus Compounds and Acetylchoinestserase

Organophosphorus compounds (OPs) are commonly used as pesticides and nerve agents. Each year, OPs poison 3,000,000 people and kill roughly 300,000.[1] Developed as a pesticide, the first OP, tabun, was synthesized by German scientist, Gerhard Schrader in the 1930's. Due to its extreme toxicity, the Germans began to develop these compounds **(**Figure 1.1) throughout World War II as nerve agents but never implemented them. After the war, OPs were rapidly studied and developed, with many countries accumulating large stockpiles of them. Since then, these compounds have been used in many conflicts around the world such as the Iran-Iraq War (1980-1988) resulting in 100,000 affected individuals. In a terrorist attack in Tokyo, sarin gas was released in the subway system, injuring thousands and resulting in twelve fatalities.[2] More recently, in 2013 OPs were used in the Syrian war civil against civilians.[3] The potency of these weapons has lead the United Nations to classify these compounds as weapons of mass destruction.[4]

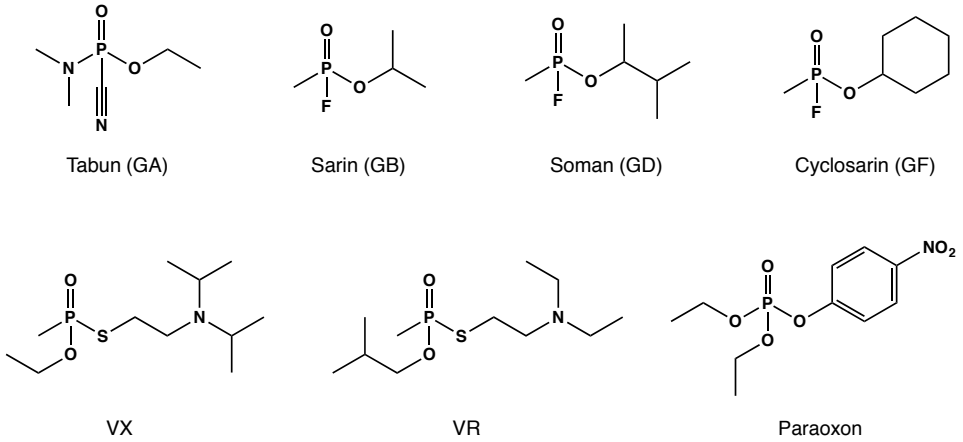

Figure 1.1: Example of OPs used as chemical weapons and the less potent pesticide, paraxon.

Because of the large threat these compounds pose, there is a pressing need for therapeutics to OP exposure. These compounds target acetylcholinesterase (AChE), an enzyme part of the central nervous system. The function of AChE is to hydrolyze the neurotransmitter acetylcholine (ACh) via the mechanism in Figure 1.2. This is important as ACh is responsible for transmitting signals activating muscle contraction.[5] However, AChE that has been inhibited by OPs are unable to do this, resulting in a buildup of ACh. Excess ACh from even mild OP exposure can lead to various symptoms such as partial blindness, convulsions, paralysis, vomiting or ultimately, death by asphyxiation at high levels of exposure. Additionally, long-term exposure may be linked to attention deficit/hyperactivity disorder and Alzheimer's disease.[6,7]

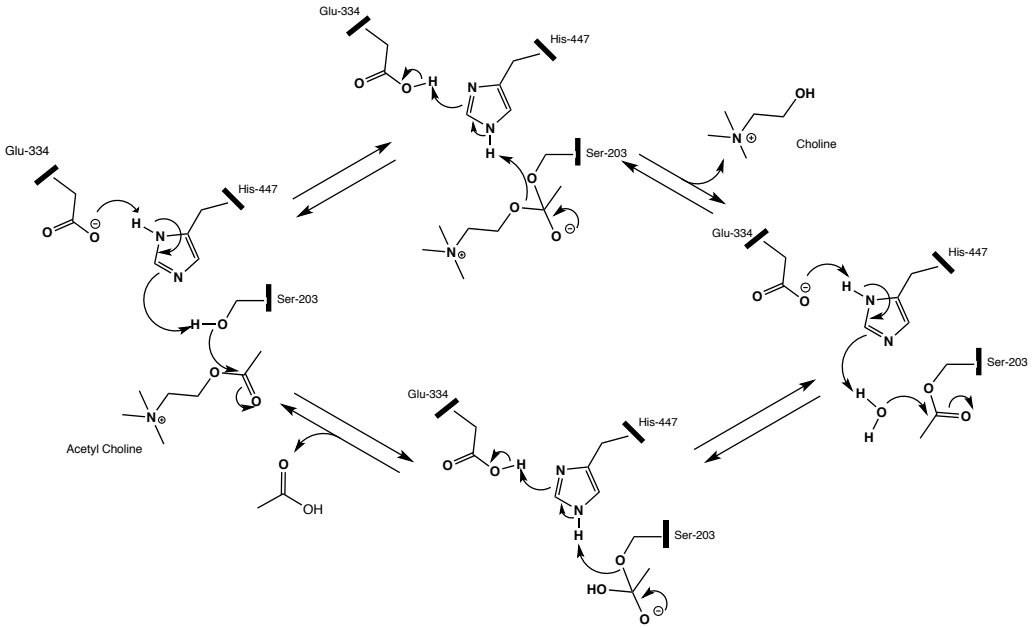

Figure 1.2: The hydrolysis of ACh via the catalytic traid (Glu-His-Ser) of AChE.

OPs inhibit acetylcholinesterase by attacking the serine residue in the catalytic triad within the enzyme active site (Figure 1.3). When exposed to OPs, the catalytic serine residue forms a covalent bond with the phosphoryl center of the OP. The OP discards its leaving group

creating a phsophonate on the serine residue, rendering the enzyme inhibited and unable to hydrolyze ACh.[8]

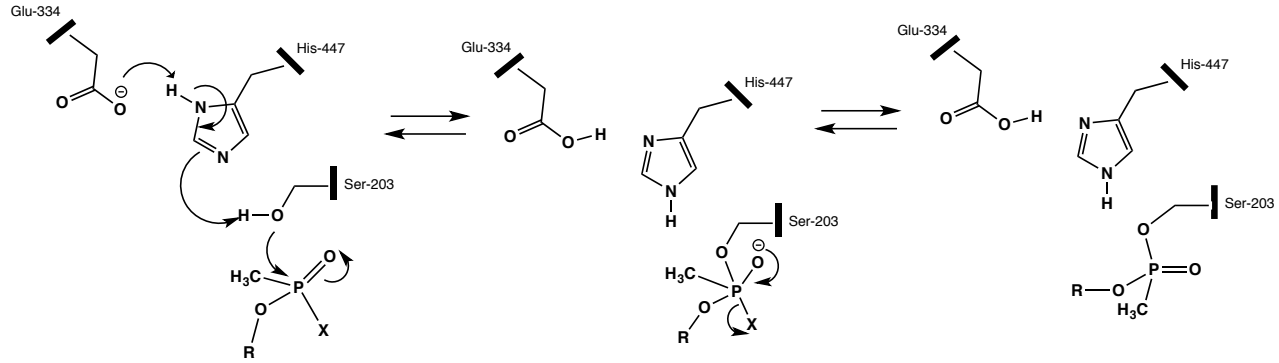

Figure 1.3: The inhibition of the catalytic Ser-203 by phosphonylation of the OP.

These phosphonates are stable and cannot be hydrolyzed to free the serine residue. There are treatments for inhibited AChE in the form of pyridinium oximes that reactivate the enzyme under certain conditions, but inhibited AChE can further undergo an aging process involving a dealkylation of the phosphonate, leaving a phophonate anion on the catalytic Ser-203 residue. Due to the lowered electrophilicity of the now stable phosphonate anion, aged AChE is resistant to therapeutic oximes leaving the enzyme inactive (Figure 1.4).[8] Currently, there are no known treatments for aged AChE, leaving those exposed to OPs at great risk.

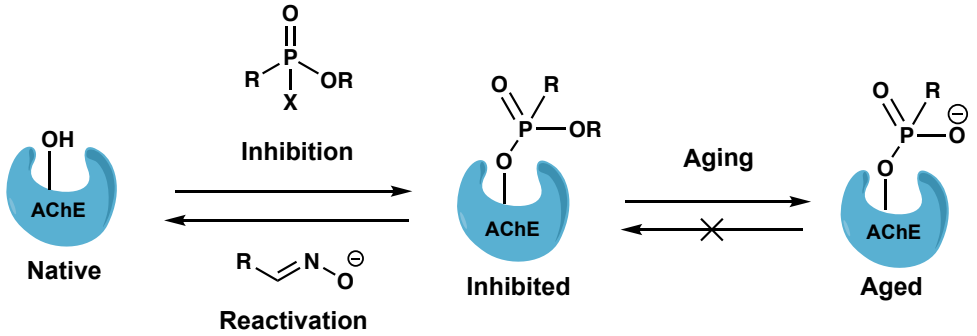

Figure 1.4: The inhibition and aging of acetylcholinesterase.

1.2 Quinone Methide Precursors as Potential Realkylating Agents

In order to realkylate a phosphonate anion, a strong electrophile is necessary. Previous literature has shown quinone methide precursors (QMPs) to be potent realkylators, especially of biological molecules. A study done by Modica et al. showed that QMPs could form a stable quinone methide (QM) and realkylate amino acids (Figure 4).[9] Additionally, quinone methides have demonstrated the ability to realkylate phophodiester bonds of DNA under physiological conditions.[10] Considering the structural similarities between phosphodiesters and the phophonate anion on aged AChE, QMs are of great interest as therapeutics for aged AChE.

As shown in Figure 1.5, QMPs will eliminate their cationic amine group upon heating or excitation to form the reactive QM intermediate, a very strong electrophile. This behavior is useful in that these compounds could potentially be delivered in their inactive form. QMPs are also of great interest because of their specificity. Past studies have shown QMPs to have tunable reactivity by altering the leaving group[11] and ring substituents.[12]

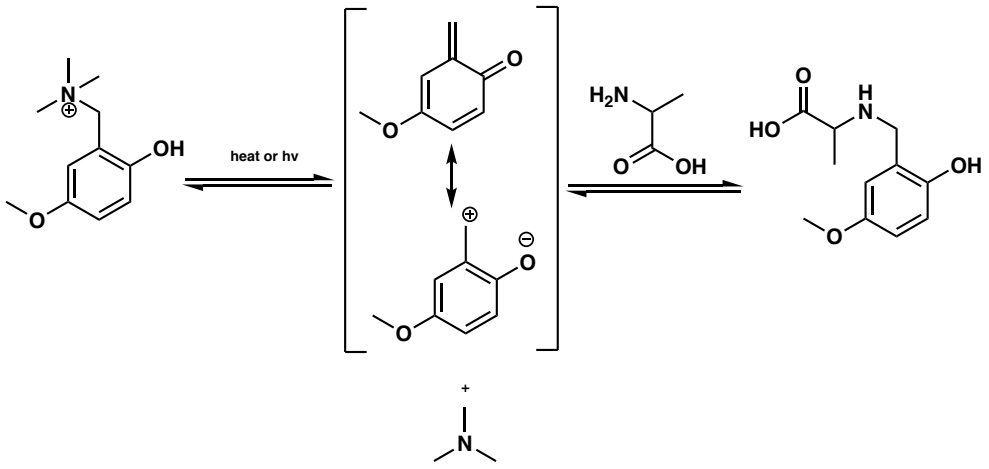

Figure 1.5: A QMP realkylating an amino acid through a QM intermediate.

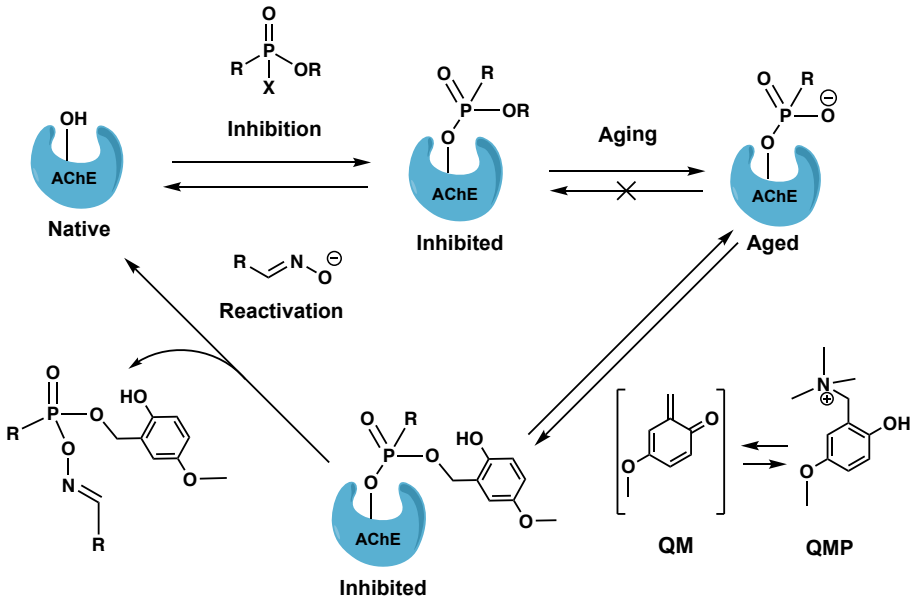

Figure 1.6: The inhibition and aging of AChE from OP exposure, subsequent realkylation by a QMP, and reactivation with oximes.

Synthetic efforts are currently employed to create QMPs for *in vitro* screening of these compounds as aged AChE realkylators. To aid in this, computational studies of QMPs have been performed to identify ideal target compounds for experimental studies. This collaboration has resulted in a few compounds that demonstrated *in vitro* resurrection of aged AChE. Each of these compounds is a variant of the substituted pyridinol in Figure 1.7, named RD-o-5. As a large number of QMPs have been studied, QMP-like compounds similar to RD-o-5 have been studied *in silico* as potential realkylators of aged AChE.[13]

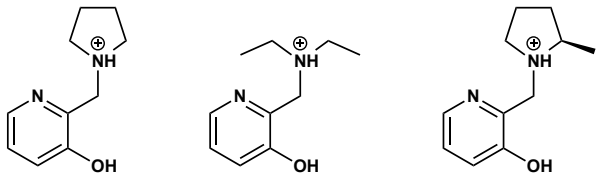

Figure 1.7: RD-o-5 (left) and other derivative that have successfully demonstrated realkylation.

1.3 References

1. Peter, M.G. *Angew. Chem. Int. Ed. Engl*. **1989**, *28*, 555.

2. Soltaninejad, Kambiz; Shahin, Shadnia. (2014). *Basic and Clinical Toxicology of Organophoshporus Compounds.* Springer London.

3. Rogin, J. Exclusive: U.S. to Bring Chemical Weapons Witnesses Out of Syria. The Daily Beast, May 2013, http://www.thedailybeast.com/articles/2013/05/22/exclusive-u-s- to-bring-chemical-weapons-witnesses-out-of-syria.html (accessed Feb 12th, 2017)

4. Security Council Resolution 687, S/RES/687 (8 April 1991) available from www.un.org/Depts/unmovic/documents/687.pdf

5. Botos, I.; Wlodawer, *A. Curr. Opin. Struct. Biol*. **2007**, *17,* 683-690.

6. Ember, L. Chemical weapons: plans prepared to destroy Iraqi arms. *Chemical and Engineering News* **1991**, 69 (33), p 6.

7. Masuda, N.; Takatsu, M.; Morinari, H.; Ozawa, T. *Lancet*. **1995**, 345, 1446.

8. Michel, H. O., Hackley, B. E. Jr, Berkowitz, L., List, G., Hackley, E. B., Gilliam, W. and Paukan, M. (1967) "*Aging and dealkylation of soman (pinocolylmethyl-phosphonofluoridate)-inactivated eel cholinesterase*." Arch. Biochem. Biophys. *121*, 29-34.

9. Modica, E.; Zanaletti, R.; Freccero, M.; Mela,M. *J. Org. Chem*. **2001**, *66*, 41

10. Bakke, B. A.; McIntosh, M. C.; Turnbull, K. D. *J. Org. Chem*. **2005**, *70*, 4338-4345

11. Weinert, E. E.; Dondi, R.; Colloredo-Melz, S.; Frankenfield, K. N.; Mitchell, C. H.; Freccero, M.; Rokita, S. E. *J. Am. Chem. Soc*. **2006**, *128*, 11940-11947.

12. Freccero, M. *Org. Chem.* **2004**, *1*, 403-415.

13. Zhaung, Q., Ph.D. Dissertation, The Ohio State University, 2017.

2. Library 1: Protonated 5-member Ring Heterocycles

2.1 Introduction

Due to the singular success of RD-o-5, non-pyridinol compounds with similar properties as RD-o-5 were studied *in silico*. A library of compounds with 5-member ring frameworks was chosen with similar stereochemistry as RD-o-5. Each compound has a varying heteroatom or substitution from the others (Figure 2.1). The current lead compound, RD-o-5, was also studied with this library for comparison. A methyl group on the heteroatom of the pyrrole compounds was added for synthetic viability and stability. The compounds were initially studied in their protonated forms, do to the similarity to the native ligand's choline moiety.

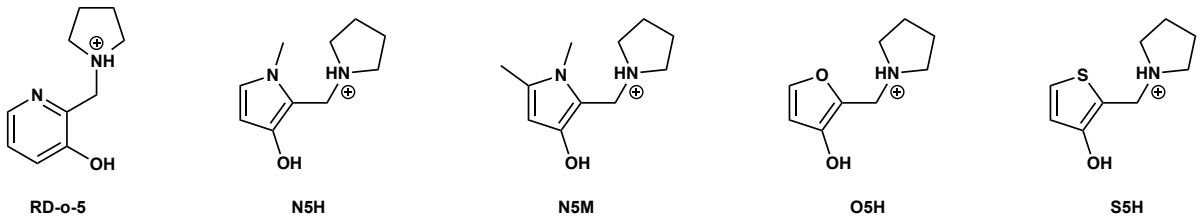

Figure 2.1: Library 1, five-member ring QMP's with varying heteroatoms.

2.2 Methodology

The methodologies used throughout these studies consisted of molecular docking of the compounds into an aged crystal structure of AChE and subsequent molecular dynamics on the generated docking poses. In order to prepare the molecules for this procedure, the compounds of interest were built in GaussView 4.1.2.[1] For each compound, several plausible conformations were made to increase the likelihood of finding the global minimum. Each of these conformations was optimized with frequency analysis using Gaussian 09[2] with a B3LYP/6-311+G** basis set and a Polarizable Continuum Model[3] of Solvation of water. The lowest energy conformation was chosen as the global minimum and checked with frequency analysis for the lack of imaginary frequencies to confirm the geometry as a minimum on the potential energy surface. For docking preparation, Merz-Kollman charge calculations were performed on the global minimum geometries of each compounds with a B3LYP/6-311+G** basis set in Gaussian 09.[2]

The compounds of interest were then analyzed with Molecular Docking. Molecular Docking was used to indicate the orientations within AChE that the ligands prefer thermodynamically through electrostatic interactions. The ligand was allowed to move freely rotationally and torsionally, whereas the receptor was held rigid, including all of the residue side chains. For the receptor, thirteen snapshots (frames) of artificially aged human AChE were used that had been prepared by Dr. Jeremy Beck.[4] These frames are stills taken from 5 nanosecond molecular dynamics simulation of aged AChE that contained a QMP in the active site. While using these frames for docking may have positively biased results due to a larger opening in the active site, it is useful because it simulates induced fit effects of AChE from QMPs despite a

rigid receptor. The initial crystal structure of AChE was obtained from the Protein Data Bank (PDB id 1B41[5]), and water, cofactors, and an associated fasciculin-II peptide were removed with UCSF Chimera.[6] Missing residues were replaced with electric ray AChE homology (PDB 1C2B[7]), and preparation was completed by aging the structure with a methyl phosphonate on the catalytic Serine-203 residue.

The prepped compounds were docked into all thirteen frames of the receptor using Autodock 4.0.[8] For efficiency, the calculations were limited to a 50 × 50 × 50 Å grid box centered at the active site, which limited the scope to the active site and its entrance (gorge mouth and bottleneck). In each receptor frame, 200 orientations (poses) of each compound in were generated (2,600 total orientations per compounds). These poses were organized on a histogram from lowest binding energy to highest binding energy (most favorable to least). Poses with similar orientation and binding energy were organized into bins (clusters). The three lowest energy clusters were analyzed for favorable interactions with the receptor; special attention was given to the distance between the benzylic carbon and the phosphonate oxygen on the aged serine residue as this is the bond that forms during the proposed realkylation event.

To study the ligand-receptor interaction more in-depth, Molecular Dynamics (MD) simulations were performed on the docking poses. MD allows the ligand and the receptor to interact over time, in a solvated environment, and with a flexible receptor. These parameters allow for a stronger simulation of what might actually happen *in vitro* than docking. An orientation from each of the three lowest-energy clusters for each compounds for each frame were used as the starting point for the simulations for a total of 39 simulations per compound. These simulations were performed with the Sander module in AMBER11.[9] The complex was

solvated with explicit water and neutralized with Na^+ ions, followed by two minimization sets to bring the system close to its global minimum. The first set used 500 steps of Steepest Descent Minimization.[10] This involves following the steepest derivative on the potential energy surface away from any local maximum very quickly. This was followed by 500 steps of a Conjugate Gradient Minimization[10], which lowers the system's energy similarly to Steepest Descent Minimization, but more slowly for a greater degree of accuracy. For the second set of minimizations, 1000 steps of Steepest Descent Minimization proceeded by 1500 steps of Conjugate Gradient Minimization were performed on the system. To conclude the preparation, the system was heated linearly from 0 Kelvin to 300 Kelvin over 20 picoseconds (10,000 steps of 2 femtoseconds) at 1 atm. Finally, MD calculations of 1 nanosecond (500,000 steps of 2 femtoseconds) were performed for each pose.

Following the completion of these calculations, the simulations were visualized and studied in Visual Molecular Dynamics.[11] Various interactions and relationships between the ligand and the receptor were analyzed qualitatively and quantitatively.

2.3 Enol Stability and Tautomerization

One concern with these compounds is their affinity for their keto-tautomers. Both the keto tautomers (Figure 2.2) were optimized with the parameters describes in Section 2.2. Their relative stabilities are shown in Table 2.1. For the keto-tautomers, the most stable enantiomer was used (R in all cases). The relative energies show that the keto form is heavily favored thermodynamically. Conversely, RD-o-5 is most stable in its enol form by 20.75 kcal/mol. Gas phase optimizations were also performed on the enol structures to verify this results (Table 2.2). For each compound, the keto form was still favored, though the stability gained was reduced by ≈1-2 kcal/mol. The structural reasons for keto favorability will be further explored in Chapter 3. However, even though the enol form is disfavored for Library 1 and the keto forms cannot form QMs, these compounds were still studied in order to observe how changes in framework affect active site interactions and for the possibility that tautomerization can occur in the active site.

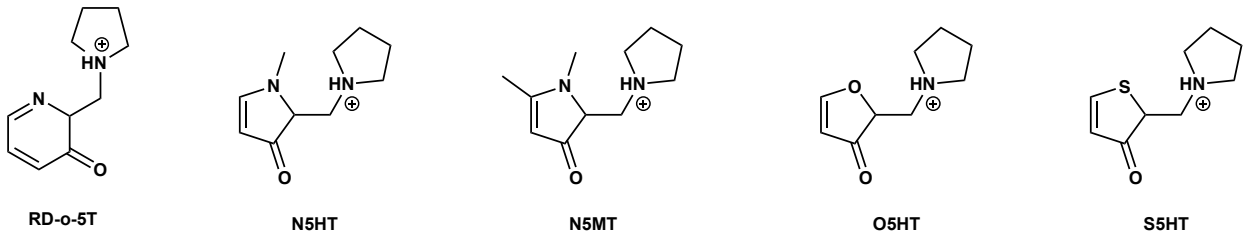

Figure 2.2: The respective keto-tautomers of Library 1.

Table 2.1: The relative stabilities of Library 1 and their respective tautomers (solvated)

Ligand	Relative Enol Stablity (kcal/mol)	Relative Keto Stablity (kcal/mol)
N5H	0.00	-5.31
N5M	0.00	-8.66
O5H	0.00	-5.66
S5H	0.00	-2.63
RD-o-5	**-20.75**	0.00

Table 2.2: The relative stabilities of Library 1 and their respective tautomers (gas phase)

Ligand	Relative Enol Stability (kcal/mol)	Relative Keto Stability (kcal/mol)
N5H	0.00	-3.00
N5M	0.00	-6.46
O5H	0.00	-4.25
S5H	0.00	-1.34

2.4 Molecular Docking Results

The docking results were analyzed with focus on benzylic carbon – phosphonate oxygen (BC-PO) distance. For each pose the BC-PO distance was measured, and the pose was sorted accordingly. The results are summarized in the histogram in Figure 2.3, where the amount of poses that have a BC-PO within specified ranges are grouped together to form a distribution. Specific BC-PO distances also correspond to various locations within the active site and gorge. These are defined in Table 2.3, and the percent of poses each compounds binds to a specific region are shown in Table 2.4.

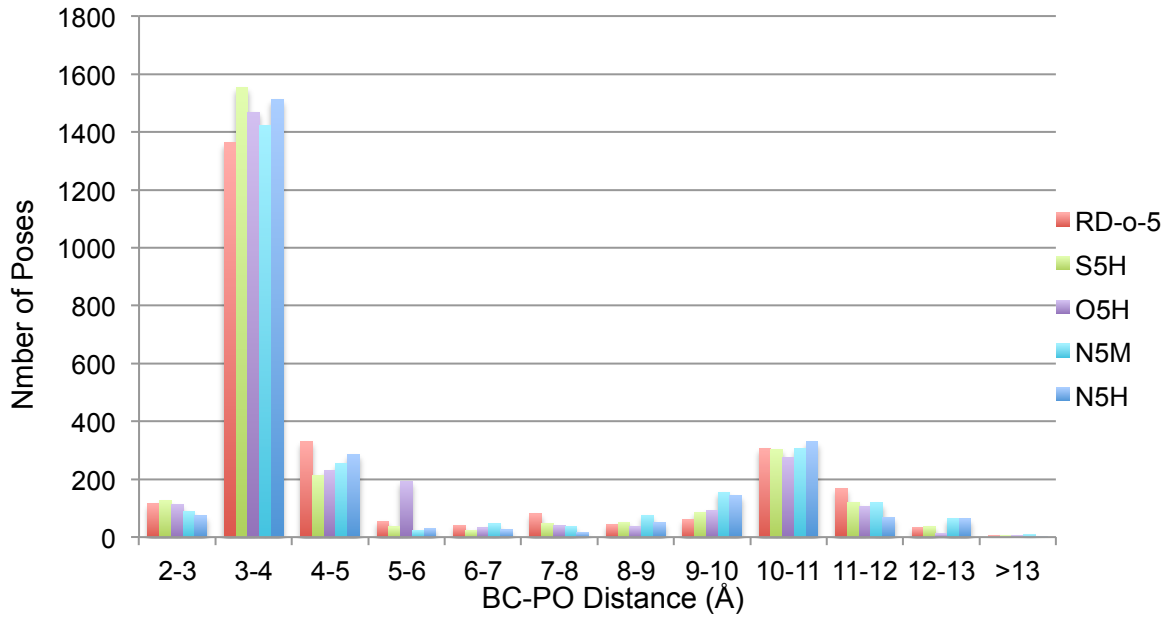

Figure 2.3: The distribution of the distance of each ligand to the aged serine residue.

Table 2.3: Defined zones of AChE

Zone	Active Site (AS)	Between AS and BN	Bottleneck (BN)	Between BN and GM	Gorge Mouth (GM)
Distance from Ser-203	0-5Å	5- 7 Å	7 - 9.5 Å	9.5 Å - 10 Å	10 - 15 Å

Table 2.4: Percent of poses ligands spends in each region of aged AChE

Ligand	% Active Site	% Between AS and BN	% Bottleneck	% Between BN and GM	%Gorge Mouth
N5H	72	2	6	2	18
N5M	68	3	6	4	19
O5H	70	9	5	2	15
S5H	73	2	5	2	18
RD-o-5	70	4	6	1	20

All ligands performed similarly in terms of active site affinity, at the same level as RD-o-5 or better. Based on docking alone, it appears that ring scaffold itself has little effect on the active site affinity, seeing that the distribution was very similar across all five ligands. Though marginally small, N5M spent the least amount of poses in the active site. This is likely due to the fact that the added methyl group hinders favorable hydrogen bonding interactions within the active site and gets stuck in the gorge mouth, unable to bypass the bulky aromatic residues like Phe-295, Phe-296 and Phr-338 (Figure 2.4). In contrast, N5H is more able to form a salt bridge with the phosphonate anion and hydrogen bond to Glu-202.

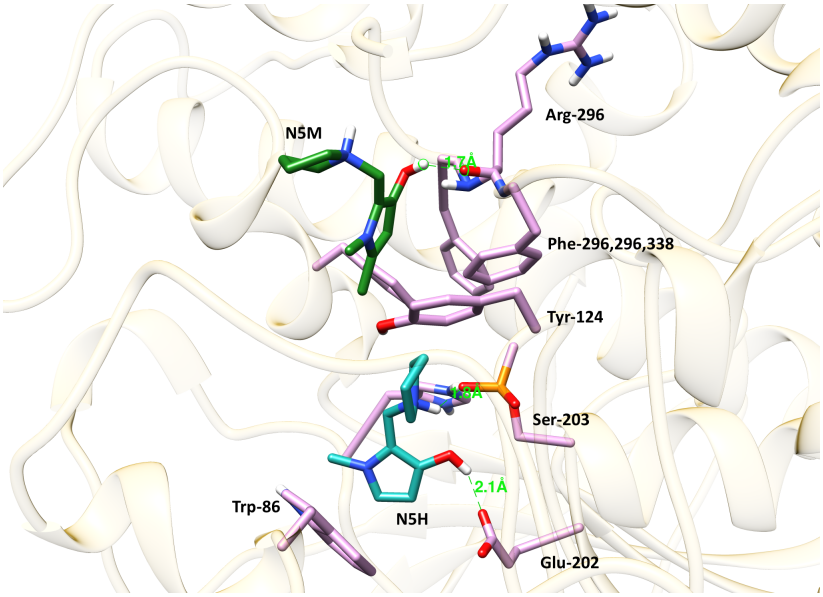

Figure 2.4: Most stable conformations of N5M (top) and N5H (below), hydrogen bonds shown in green.

Another small but significant discrepancy is that despite RD-o-5 spending as much time in the active site (within 5 Å) as the other ligands, it spends the least amount of poses within 4 Å. This is due to greater interaction with Trp-86. With a larger π-system than the 5-member ring ligands, RD-o-5 more readily forms π-π interactions with Trp-86, which holds the ligand near 5 Å (Figure 2.5). These findings were augmented in MD, where the interactions were studied in more detail.

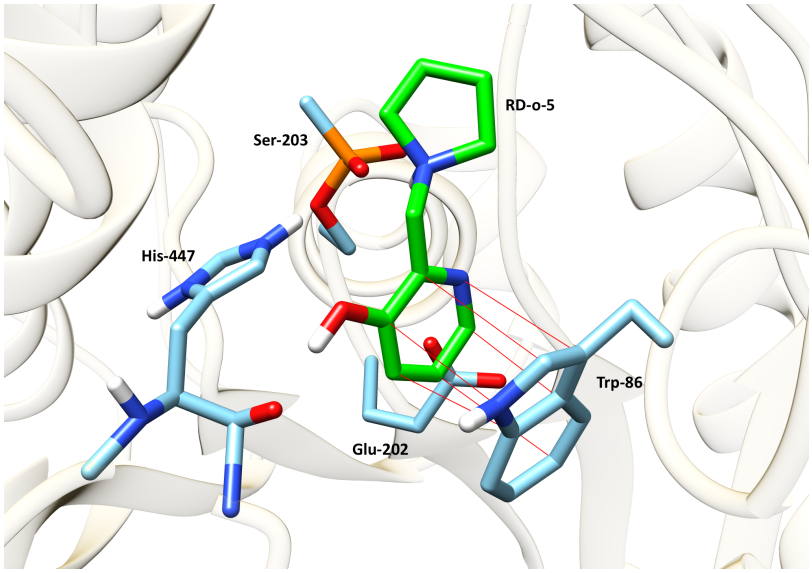

Figure 2.5: RD-o-5 π-stacking with Trp-86.

2.5 Molecular Dynamics Results

MD allowed for the enzyme ligand interactions to be more thoroughly examined. As with docking, the BC-PO distance was measured and analyzed and the data was characterized by the percent of time the ligand spends in each region of AChE (Table 2.5) (For MD simulations, the active site range was extended to 6 Å BC-PO distance). Similar to the docking results, most of the ligands performed as well or better than RD-o-5 with the exception of N5M which performed considerably worse. In addition to the benzyllic carbon displacement, several other measurements were made during the simulations (Table 2.6 & 2.7).

Table 2.5: Distribution of benzylic carbon displacement from phosphonate over time.

Ligand	% Active Site	% Between AS and BN	% Bottleneck	% Between BN and GM	% Gorge Mouth
N5H	76	7	5	2	10
N5M	**65**	6	7	2	**19**
O5H	**76**	9	4	0	9
S5H	78	5	8	1	9
RD-o-5	71	11	6	1	8

Table 2.6: Percent of time ligand hydrogen bonds to key residues (within 2.5 angstroms unless otherwise noted).

Ligand H-Bond Donor	% Phosphonate Oxygen	% Glu-202 Oxygen	% Tyr-337 Oxygen (3.5 Å)
N5H Ammonium	8	**63**	2
N5H Hydroxy	**36**	20	**9**
N5M Ammonium	22	50	1
N5M Hydroxy	**27**	24	6
O5H Ammonium	11	**56**	3
O5H Hydroxy	13	43	2
S5H Ammonium	20	50	3
S5H Hydroxy	25	32	4
RD-o-5 Ammonium	16	48	3
RD-o-5 Hydroxy	22	40	2

Table 2.7: Aromatic interactions with Trp-86.

Ligand	% π- π W-86 (4.5)	% Cation-π (5 Å)	% Cation-π (4.5 Å)
N5H	15	28	11
N5M	4	26	10
O5H	36	47	17
S5H	26	36	19
RD-o-5	30	40	21

One key interaction observed in docking that was not conserved during MD was hydrogen bonding to Tyr-337, with only N5H showing a vague affinity for the residue. Instead, the ligands preferred to hydrogen bond directly to the aged phosphonate residue and the likewise negatively charged Glu-202 beneath it. In particular, the ammonium substituent strongly favored forming salt bridges with Glu-202, positioning the compound well for a S_N2 back attack (Table 2.6).

The worst performing ligand, N5M, also spent the least percent of time interacting with W-86. Similarly, N5H also spent little time involved in π-interactions. Observation of the simulation shows that the two-methyl groups on N5M interfere with its ability for π-π interaction with W-86 (Figure 2.6) This could also be the case for N5H, though it only has one methyl group. With π-π interactions limited, when the ligands were in the active site they were often pulled closer to the negatively charged phosphonate and Glu-202. These two ligands spent the most time hydrogen bonding and forming salt bridges with either the phosphonate and or Glu-202 because of this (Table 2.6). Table 2.8 shows that although N5H and N5M might spend less time in the active site area (within 6 Å), they tend to be closer to the target residue (within 4 Å). Similar to docking, N5M spent the most time in the gorge mouth but by a far greater margin, unable to overcome steric hindrance during the simulation. N5M often interacted with a loop in

the gorge mouth including some hydrogen bonding interactions with Arg-296, Phe-295, Phe-338, and Tyr-341.

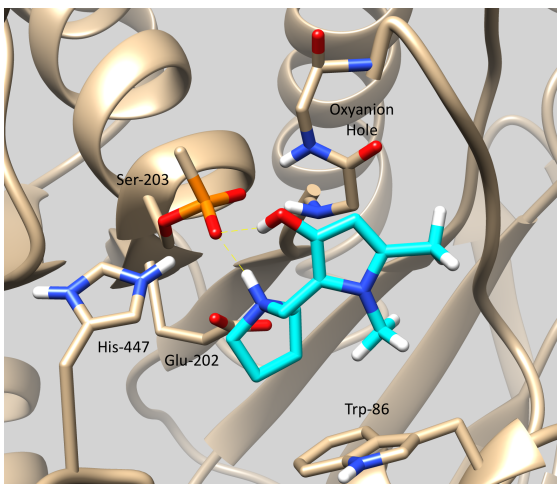

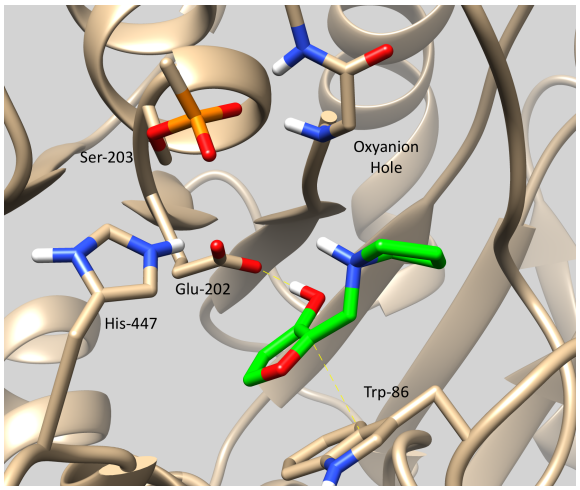

Figures 2.6 & 2.7: N5M (left) and O5H (right) in the active site of aged AChE.

Table 2.8: Percent time benzylic carbon is within 4 Å of the aged residue.

Ligand	% <4 Å	% <6 Å	% >10 Å
N5H	**56**	76	10
N5M	**50**	**65**	**20**
O5H	34	76	10
S5H	44	78	9
RD-o-5	36	71	11

Unlike docking, more π-interaction was displayed from the 5-member ring ligands in MD (Table 2.7). The furan derivative, O5H, was particularly apt to show π-π and cation-π interactions with Trp-86. This is likely why it spent the most time in the active site, yet spent the least percent of time within 4 Å of the phosphonate. Trp-86 often suspended the ligands between it and phosphonate with the hydrogen bond donor substituents naturally facing the phosphonate with ring toward Trp-86 (Figure 2.7).

After examining these interactions, it is evident why RD-o-5 works well within the active site compared to other pyridinol-QMPs. One of the most common poses involved both hydrogen bond donors simultaneously interacting with either the phosphonate or Glu-202 (Figure 2.8). Para-QMPs are not able to accomplish this due to having the substituents on opposite sides of the ring, resulting in weaker hydrogen bonding and perhaps interference with π-π interaction. In addition, some para-QMPs are in equilibrium with their keto-tautomer form, whereas RD-o-5 is very stable in its enol form due to the resonance of the pyridine. While most of the Library 1 showed affinity equal to that or stronger than RD-o-5, which has experimentally shown realkylation, their instability and the practical synthetic challenges they pose cast doubt on their potential as good realkylators. Nevertheless, there is some worth in exploring their experimental possibilities. Particularly, N5H shows promise as it showed a high affinity for the active site in addition to having very close interaction (within 4 Å) with the phosphonate.

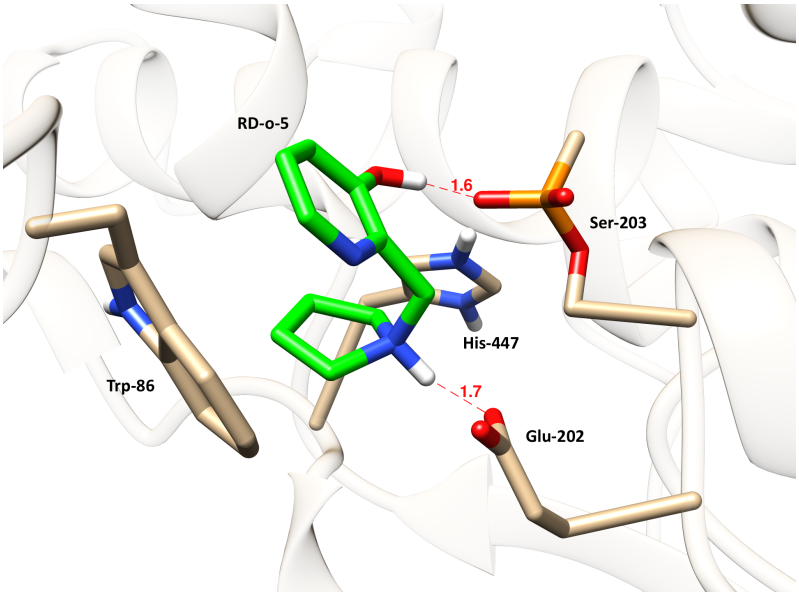

Figure 2.8: RD-o-5 (green) simultaneously hydrogen bonding (red) with Ser-203 and Glu-202.

2.6 References

1. GaussView, Version 4.1.2, Dennington, Roy; Keith, Todd; Millam, John. Semichem Inc., Shawnee Mission, KS, 2009.

2. Gaussian 09, Revision D.01, Frisch, M. J.; Trucks, G. W.; Schlegel, H. B.; Scuseria, G. E.; Robb, M. A.; Cheeseman, J. R.; Scalmani, G.; Barone, V.; Mennucci, B.; Petersson, G. A.; Nakatsuji, H.; Caricato, M.; Li, X.; Hratchian, H. P.; Izmaylov, A. F.; Bloino, J.; Zheng, G.; Sonnenberg, J. L.; Hada, M.; Ehara, M.; Toyota, K.; Fukuda, R.; Hasegawa, J.; Ishida, M.; Nakajima, T.; Honda, Y.; Kitao, O.; Nakai, H.; Vreven, T.; Montgomery, J. A., Jr.; Peralta, J. E.; Ogliaro, F.; Bearpark, M.; Heyd, J. J.; Brothers, E.; Kudin, K. N.; Staroverov, V. N.; Kobayashi, R.; Normand, J.; Raghavachari, K.; Rendell, A.; Burant, J. C.; Iyengar, S. S.; Tomasi, J.; Cossi, M.; Rega, N.; Millam, N. J.; Klene, M.; Knox, J. E.; Cross, J. B.; Bakken, V.; Adamo, C.; Jaramillo, J.; Gomperts, R.; Stratmann, R. E.; Yazyev, O.; Austin, A. J.; Cammi, R.; Pomelli, C.; Ochterski, J. W.; Martin, R. L.; Morokuma, K.; Zakrzewski, V. G.; Voth, G. A.; Salvador, P.; Dannenberg, J. J.; Dapprich, S.; Daniels, A. D.; Farkas, Ö.; Foresman, J. B.; Ortiz, J. V.; Cioslowski, J.; Fox, D. J. Gaussian, Inc., Wallingford CT, 2009.

3. Mennucci, B. (2012), Polarizable continuum model. WIREs Comput Mol Sci, 2: 386–404. doi: 10.1002/wcms.1086

4. Beck, J. M., Ph.D. Dissertation, The Ohio State University, 2011.

5. Kryger, G.; Harel, M.; Giles, K.; Toker, L.; Velan, B.; Lazar, A.; Kronman, C.; Barak, D.; Ariel, N.; Shafferman, A.; Silman, I.; Sussman, J. L.Acta Crystallogr., Sect. D **2000**, *56, 1385- 1394.*

6. Pettersen, E. F.; Goddard, T. D.; Huang, C. C.; Couch, G. S.; Greenblatt, D. M.; Meng, E. C.; Ferrin, T. *E. J. Comput. Chem*. **2004**, *25,* 1605-1612.

7. Bourne, Y.; Grassi, J.; Bougis, P. E.; Marchot, J. *J. Biol. Chem.* **1999**, *274*, 30370-30376

8. Morris, G. M., Huey, R., Lindstrom, W., Sanner, M. F., Belew, R. K., Goodsell, D. S. and Olson, A. J. (2009) Autodock4 and AutoDockTools4: automated docking with selective receptor flexiblity. J. Computational Chemistry **2009**, *16*: 2785-91.

9. Case, D. A.; Darden, T. A.; Cheatham, T. E., III; Simmerling, C. L.; Wang, J.; Duke, R. E.; Luo, R.; Crowley, M.; Walker, R. C.; Zhang, W.; Merz, K. M.; Wang, B.; Hayik, S.; Roitberg, A.; Seabra, G.; Kolossváry, I.; Wong, K. F.; Paesani, F.; Vanicek, J.; Wu, X.; Brozell, S. R.; Steinbrecher, T.; Gohlke, H.; Yang, L.; Tan, C.; Mongan, J.; Hornak, V.; Cui, G.; Mathews, D. H.; Seetin, M.G.; Sagui, C.; Babin, V.; Kollman, P. A. AMBER 11, University of California, San Francisco, 2008.

10. Adcock, S. A., & McCammon, J. A. Molecular Dynamics: Survey of Methods for Simulating the Activity of Proteins. *Chemical Reviews* **2006**, *106*(5), 1589–1615. doi:10.1021/cr040426m

11. Humphrey, W., Dalke, A. and Schulten, K., "VMD - Visual Molecular Dynamics", *J. Molec. Graphics*, **1996**, *vol. 14, pp. 33-38.*

3. Library 2: Protonated Keto Tautomers

3.1 Introduction

Due to Library 1's strong preference to tautomerize, a library of the respective R and S keto tautomers (Figure 3.1) were studied in the same way to determine their affinity for the active site. It should be noted that these compounds cannot act in a QMP-like fashion due to the lack of a hydroxyl group. However, these compounds should still be considered for the possibility of tautomerization within the active site or a different mechanism of realkylation. The exact mechanism of realkylation is currently unknown, but an S_N2 pathway at the benzylic carbon with the ammonium leaving group is very plausible.

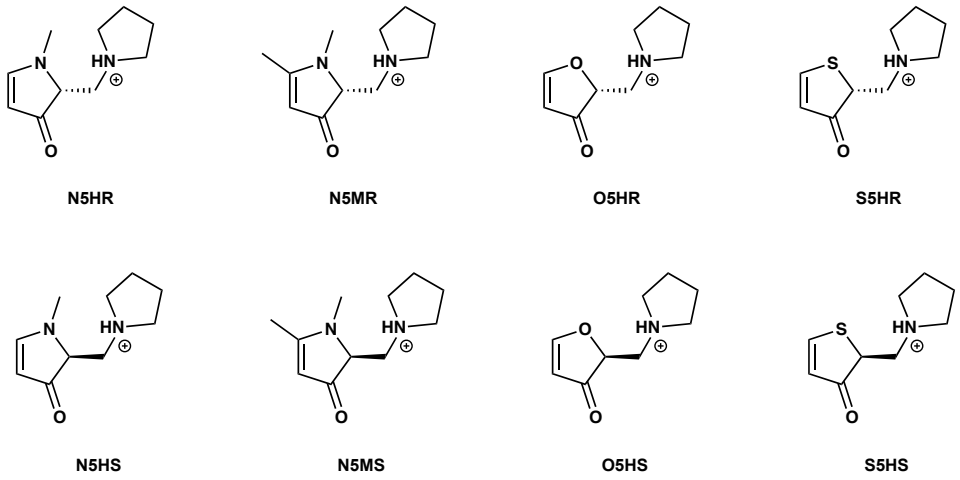

Figure 3.1: Library 2, the protonated R and S keto tautomers of Library 1.

3.2 Stability and Conformation

The keto form was preferred by each compounds by about 5 kcal/mol solvated and approximately 2 kcal/mol in the gas phase (Table 3.1) This was not predicted due to the loss of aromaticity of the keto form. Notably, S5H shows the least stability gained in the keto-form. When the geometries were analyzed it was shown that a significant contribution to the stability of the keto forms was a greater ability to hydrogen bond. The distance between the ammonium hydrogen and the nearest hydrogen bond acceptor was measured for each solvated geometry as well as the hydrogen bond angle (Table 3.2). The gas phase geometries show similar trends.

Table 3.1: The gas and solvent phase stabilities of the keto and enol tautomers.

Ligand	Solvated		Gas Phase	
	Relative Enol Stability (kcal/mol)	Relative Keto Stability (kcal/mol)	Relative Enol Stability (kcal/mol)	Relative Keto Stability (kcal/mol)
N5H	0.00	-5.31	0.00	-3.00
N5M	0.00	-8.66	0.00	-6.46
O5H	0.00	-5.66	0.00	-4.25
S5H	0.00	-2.63	0.00	-1.34

Table 3.2: Potential hydrogen bond measurements of enol tautomers

Ligand	Potential Hydrogen Bond Distance (Å)	Potential Hydrogen Bond Angle (°)
N5H*	3.16	95.7
N5M*	3.16	95.7
O5H**	3.48	107.5
S5H**	**2.20**	**130.6**
RD-o-5*	**2.11**	**128.8**

**Hydrogen bond to heteroatom*
*** Hydrgoen bond to hydroxy*

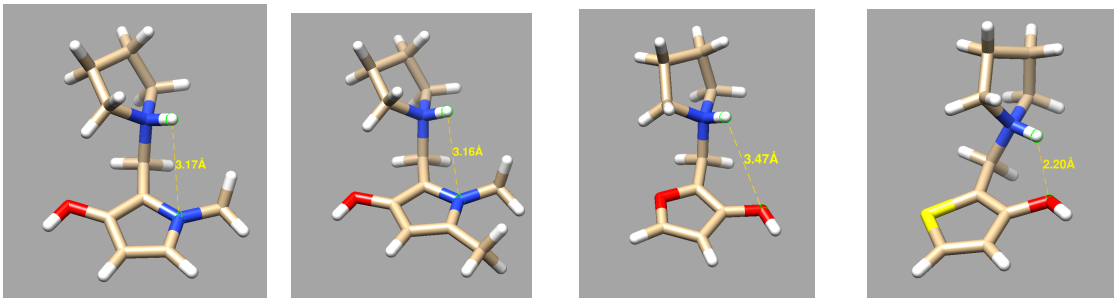

Figures 3.2-3.5: The global minima enol tautomers of Library 1.

Only S5H appears to demonstrate a weak intramolecular hydrogen bond with the hydroxyl group, accounting for the smaller relative difference in energy between tautomers. Conversely, a potential hydrogen bond in O5H is too far and too high of an angle to truly offer stability (Table 3.2). Both pyrrole compounds adopt a conformation where the ammonium hydrogen bond donor points to the heteroatom on the ring, but does not display a true hydrogen bond. This conformation may be favorable for the pyrrole compounds due to the possible increase of steric hindrance between the benzylic hydrogen, pyrrolidine and the methyl group on the heteroatom. However, the greater flexibility of the keto compounds allows for hydrogen bonding to occur more easily (Figure 3.6). Each keto compound shows a smaller hydrogen bond distance and a more favorable hydrogen bond angle than their enol counterparts (Table 3.3).

Table 3.3: Hydrogen bond measurements of keto tautomers.

Ligand	Hydrogen Bond Distance (Å)	Hydrogen Bond Angle (°)
N5HR	1.83	145.2
N5HS	1.84	144.5
N5MR	1.82	145.4
N5MS	1.82	145.4
O5HR	1.96	141.4
O5HS	1.98	141.4
S5HR	1.91	141.0
S5HS	1.92	140.3

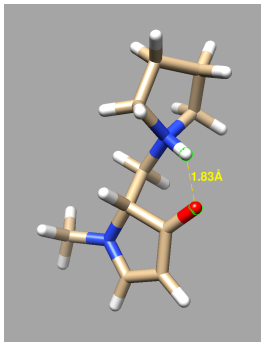

Figure 3.6: The global minimum keto form of N5HR shows ease of hydrogen bonding.

To study the magnitude of the effect of hydrogen bonding, two conformations of each keto compound were compared: a conformation with intra-molecular hydrogen bonding (conformation 1, the global minimum, Figure 3.6) and the next most stable conformation without a hydrogen bond (conformation 2, Figure 3.7). The results are summarized in Table 3.4. The keto tautomers strongly favored intramolecular hydrogen bonding to the hydroxy group which stabilized the structure by ~3 kcal/mol. This accounts for much of the energy difference between the tautomers. Additionally, steric strain from an unfavorable 5-member ring is relieved by the added flexibility at the chiral sp^3 carbon. This would result in greater stabilization of a more sterically strained compound, which could be the case for N5M. Seeing that RD-o-5 already lacks steric strain and has strong hydrogen bond capabilities in the enol form, it is reasonable that it would prefer the enol form and maintain aromaticity.

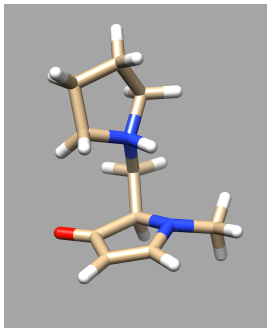

Figure 3.7: Conformation 2, the most stable conformation without hydrogen bonding.

Table 3.4: Energetic favorability of intramolecular hydrogen bonding

Ligand	Chirality	Conformation	Relative Energy (kcal/mol)
N5H	R	1	-3.72
		2	0.00
	S	1	-3.71
		2	0
N5M	R	1	-3.64
		2	0.00
	S	1	-3.63
		2	0.00
O5H	R	1	-2.29
		2	0
	S	1	-2.27
		2	0.00
S5H	R	1	-3.18
		2	0
	S	1	-3.25
		2	0.00

**Conformation 1= hydrogen bond to hydroxy*
**Conformation 2= hydrogen bond to heteroatom*

3.3 Molecular Docking Results

The same docking procedure outlined in Chapter 2.2 was applied to Library 2. Once again, the BC-PO distance was measured for each docking pose, which sorted the poses by BC-PO distance range into distribution. Comparisons of the docking results between both keto forms and the enol form for each framework are shown in Figures 3.8-3.11.

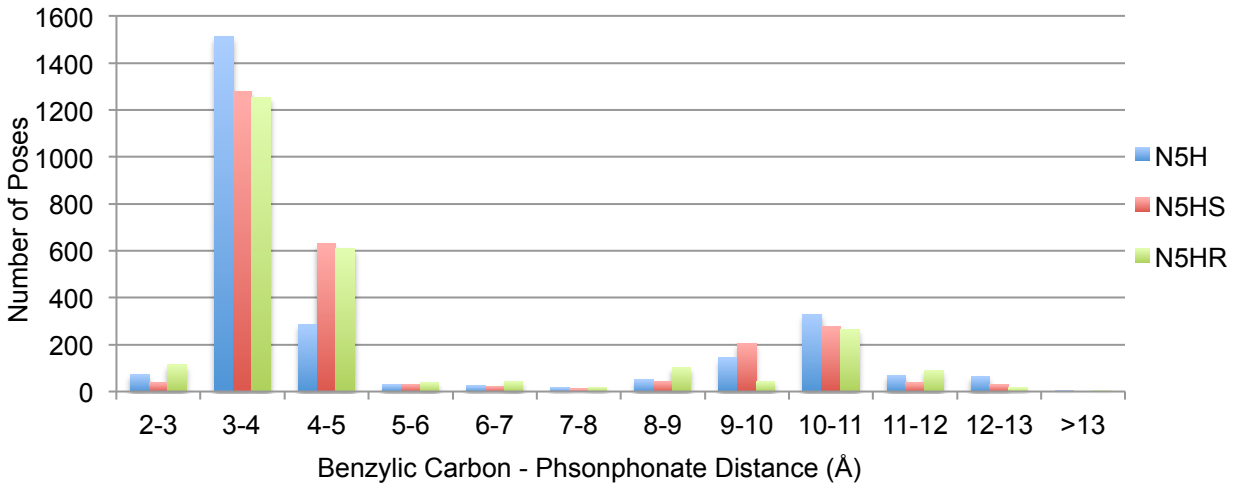

Figure 3.8: BC-PO distance distribution of N5H and its keto tautomers.

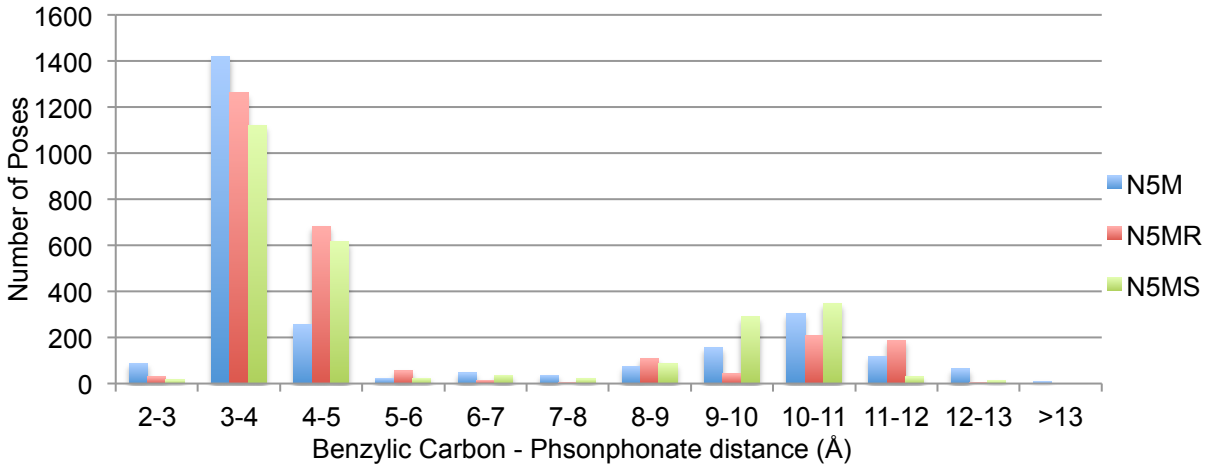

Figure 3.9: BC-PO distance distribution of N5M and its keto tautomers.

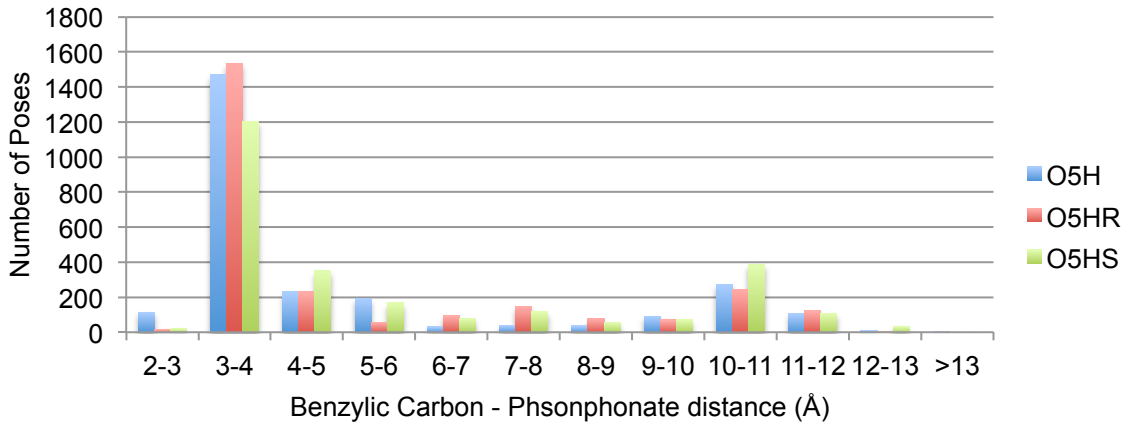

Figure 3.10: BC-PO distance distribution of O5H and its keto tautomers.

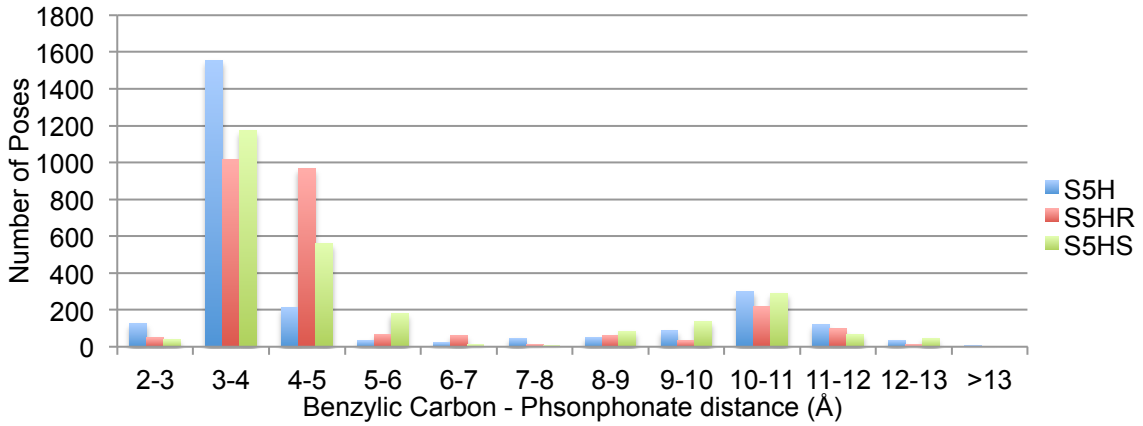

Figure 3.11: BC-PO distance distribution of O5H and its keto tautomers.

Figures 3.8-3.11 show that all keto form ligands, with exception of O5HR, had fewer poses within 4 Å of the aged serine residue, but more poses between 4 and 5 Å of the aged serine residue compared to their enol counterparts. A significant factor is the absence an extra hydrogen bond from a hydroxyl group. For the enol tautomers, the hydroxyl group allowed for key interactions with Glu-202 and the aged serine residue, which drew the ligand close to the phosphonate. Without the extra hydrogen bond donor, the keto forms were often observed interacting with other residues like π-π stacking with Trp-86 and Van der Waal's (VDW) contacts

with a loop comprising resides 119-126 (includes the oxyanion hole) and the omega loop (Figures 3.12 & 3.13). A VDW contact is defined as an atom with a VDW surface within 0.4 Å of the ligands VDW surface. For example, N5HR had 12 VDW contacts with the oxyanion hole loop and 13 contacts with the omega loop, while N5H only had 7 and 8 contacts respectively due to being more strongly drawn to the phosphonate. This was a common conformation near the active site among all of the ligands.

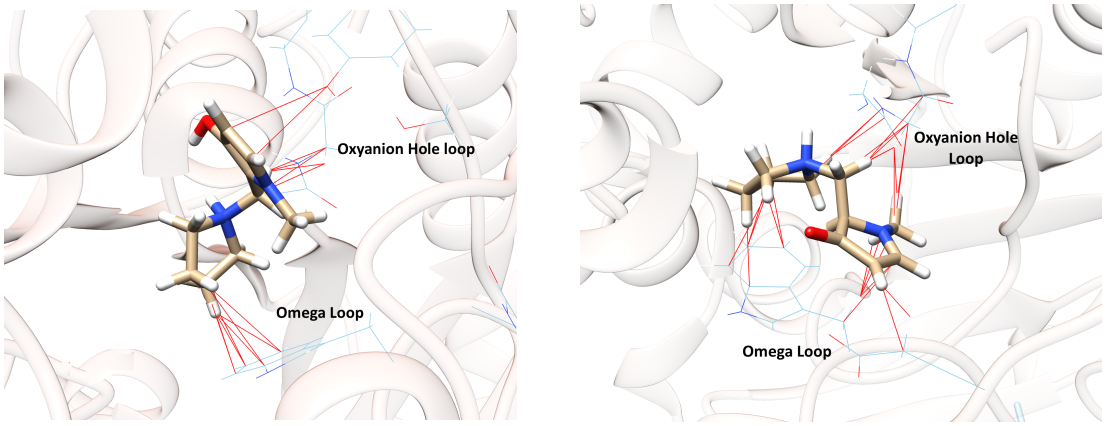

Figure 3.12 & 3.13: N5H (left) and N5HR (right) in the same frame of the active site. VDW contacts (red lines), when the VDW surface of two atoms is within 0.4 Å.

The lowest energy conformation in each frame tested (13 in total) were recorded in Table 3.5. Binding energy appears to be independent of the conformation of the ligand within the enzyme. It should be noted that N5M keto form docked into the most stable conformations in aged AChE. A likely possibility is that the methyl groups create more VDW contact to increase binding affinity, where N5MR has 34 VDW contacts with the oxyanion hole loop and Omega loops (Figure 3.14), more than N5HR at 25; demonstrating the significance of these VDW interactions. Yet as discussed with Library 1, the methyl groups could be detrimental as far as ligand orientation. This was further explored in MD simulations.

Table 3.5: Lowest binding energy conformations in each frame.

Ligand	Average Lowest Binding Energy (kcal/mol)	Lowest Lowest Binding Energy (kcal/mol)	Highest Lowest Binding Energy (kcal/mol)
N5HR	-6.1	-6.4	-5.8
N5HS	-6.2	-6.6	-5.7
N5MR	-6.6	-7.0	-6.2
N5MS	-6.5	-7.0	-5.6
O5HR	-6.0	-6.5	-6.7
O5HS	-5.9	-6.4	-5.5
S5HR	-5.7	-6.3	-5.2
S5HS	-5.8	-6.2	-5.4

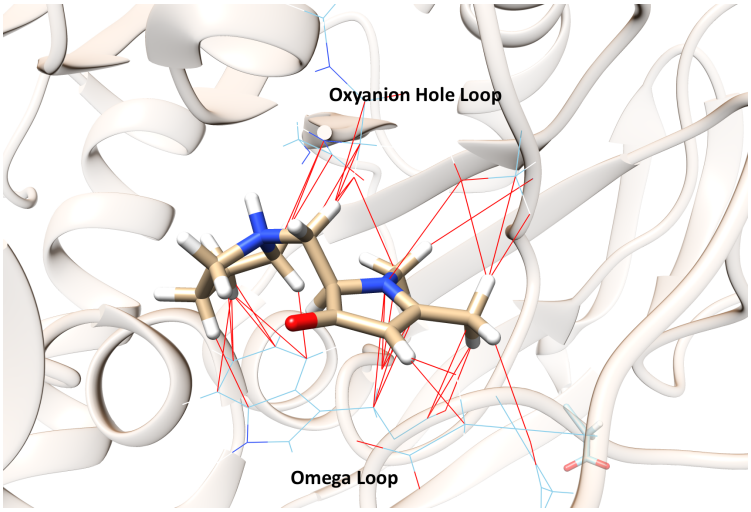

Figure 3.14: VDW contacts of N5MR within the aged AChE active site.

3.4 Molecular Dynamics Results

The MD simulations are consistent with the docking results at favoring a BC-PO distance of less than 6 Å approximately 75% of the time. However, the keto form ligands spend a relatively small percent of time within 4 Å of the aged serine residue compared to their enol counterparts reflecting the docking results. The MD simulations showed a very high favorability of the keto form ligands to a loop of residues that contains the oxyanion hole. This was analyzed by measuring the distance between the alpha carbon of Gly-121 to the centroid of the ring structure of the ligand (Figure 3.15 & Table 3.7). The affinity to this pocket held the benzylic carbons of these ligands at 4-6 Å from the phosphonate (Figure 3.16). The centroid of the ring was also measured to the centroid of Trp-86 to track π-π interaction (Table 3.7).

Table 3.6: Percent time benzylic carbon is within 4 Å of the phosphonate oxygen.

Ligand	% <4 Å	% <6 Å	% >10 Å
N5HR	21	76	12
N5HS	28	67	14
N5MR	26	77	11
N5MS	25	69	1
O5HR	22	77	13
O5HS	15	66	9
S5HR	11	84	9
S5HS	14	73	1

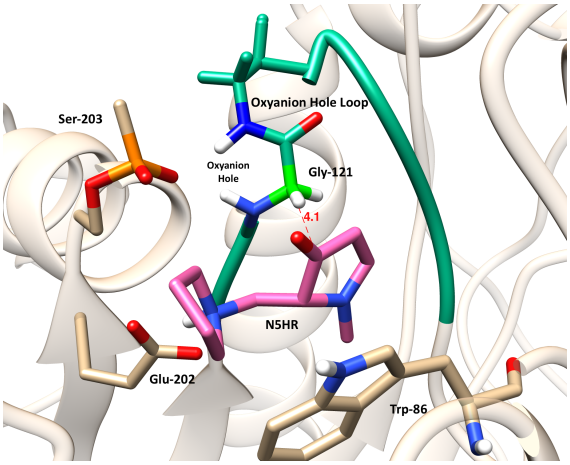

Figure 3.15: The distance from Gly-121 alpha carbon (lime green) to the ring centroid of the ligand (pink) measurement (red) near the oxyanion hole loop (teal).

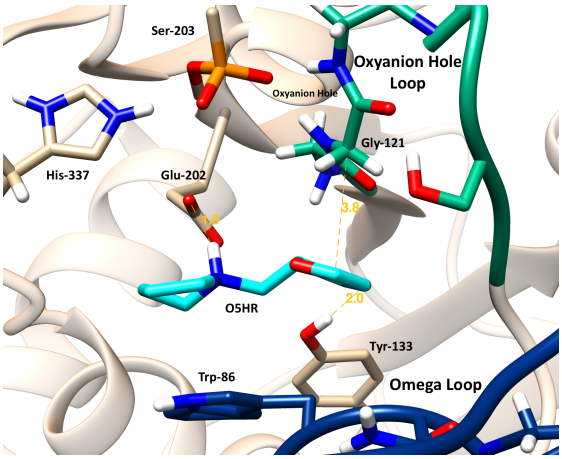

Figure 3.16: O5HR (light blue) nestled between the omega loop (navy) and oxyanion hole loop (teal).

Table 3.7: Percent time ligand ring centroid interacts with different structure.

Ligands	% Gly-121 Cα (4 Å)	% Gly-121 Cα (4.5 Å)	% π-π (4 Å)	% π-π (4.5 Å)
N5HR	34	49	15	37
N5HS	29	43	14	25
N5MR	33	61	26	43
N5MS	32	48	25	31
O5HR	28	50	4	18
O5HS	15	34	2	17
S5HR	34	57	9	32
S5HS	22	38	13	35

Trp-86 often showed edge π-π stacking in conjunction with VDW interaction with the oxyanion hole loop as the primary forces holding the ligand in place. Of these ligands, the N5M keto tautomers favored VDW and π-π interaction the most. This is in contrast to the enol-tautomers where N5M favored π-π interactions the least. This is because the methyl groups on N5M prevented π-π stacking when both hydrogen bond donor groups pulled the ligand towards the phosphonate. However, when the keto-forms favor the hydrophobic loop near the oxyanion hole, the added methyl groups create more VDW interactions with the oxyanion hole loop (particularly Gly-120, Gly-121, Gly-122), and omega loop backbone atoms (Figure 3.16). This pocket was less favorable for the enol variants due to the polarity added by an extra hydrogen bond donor on the ring. Also notable is that the R enantiomer shows more interaction with the oxyanion hole loop, but this discrepancy is not reflected in π-π interaction, particularly at more defined interactions within 4 Å.

The ketone on each ligand occasionally showed significant hydrogen bond interactions with several tyrosine residues near the active site while in the oxyanion hole loop (Table 3.8). Tyr-337 showed the most significant hydrogen bonding (Figure 3.17) over Tyr-133 (Figure 3.16) and Tyr-124. Again, the R enantiomer showed more interaction for Tyr-337. These hydrogen bond interactions may improve binding slightly but it appears that VDW forces with the relatively nonpolar pocket are the largest contributing factors to the affinity for this pocket because most of these hydrogen bond interactions occur less than a quarter of the time.

Table 3.8: Percent of time ligand carbonyl acts as hydrogen bond acceptor to tyrosine residues

Ligand	% Ty-133	% Tyr-124	% Tyr-337 (2.5 Å)	% Tyr-337 (3 Å)
N5HR	3	3	17	24
N5HS	6	4	8	13
N5MR	5	2	31	36
N5MS	8	5	11	14
O5HR	7	0	9	16
O5HS	6	3	2	4
S5HR	0	0	7	13
S5HS	7	0	6	11

**Considered hydrogen bond if less than 2.5 Å unless noted*

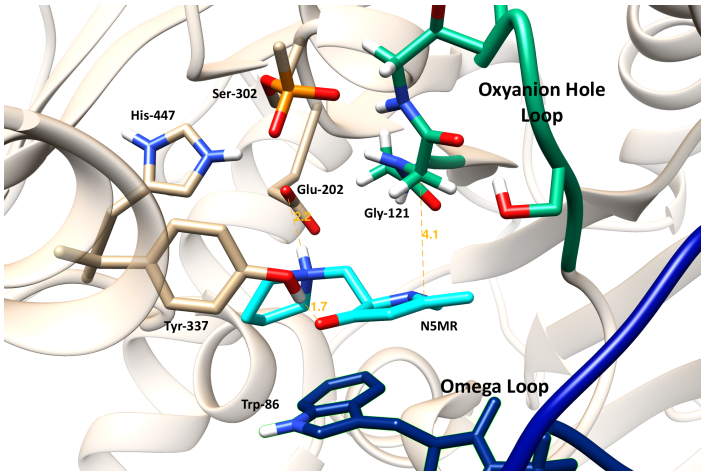

Figure 3.17: Tyr-337 hydrogen bonding to the carbonyl group of N5MR (light blue) while the ring is nestled between the omega loop (navy) and the oxyanion hole loop (teal)

Similar to the enol tautomers, the keto forms favored hydrogen bonding to Glu-202 rather than the phosphonate but to a greater extent, where no keto-tautomers hydrogen bonded to the phosphonate more than 16 % of the time (Table 3.9). This is because hydrogen bonding to Glu-202 more readily allows for VDW interactions with the oxyanion hole loop. The thiophene and furan compounds show the greatest affinity for this residue likely due to fewer VDW with the oxyanion hole loop that can pull the ligands away from Glu-202. Notably, the levels of cation-π

interaction are about the same as observed for the enol compounds. As the ammonium was often suspended between Trp-86 and Glu-202, cation-ip interaction should remain the same if salt bridges with Glu-202 are still being formed.

Table 3.9: Percent time ammonium nitrogen hydrogen bonds or has cation-π interaction.

Ligand	% H-Bond to Phosphonate Oxygen	% H-Bond to Glu-202	% Trp-86 Cation-π (4.5 Å)
N5HR	6	44	9
N5HS	16	51	17
N5MR	16	49	15
N5MS	10	45	22
O5HR	12	61	19
O5HS	4	63	23
S5HR	7	71	16
S5HS	7	59	19

Until now, the distinction between R and S enantiomers has not been mentioned. The MD simulations show a distinct difference in performance between the R and the S enantiomers for each ligand. In all cases, the R enantiomer spends more time within 6 angstroms of the phosphonate as well as more time interacting with the oxyanion hole loop (Table 3.6 and 3.7). Although there is a numerical difference, the exact orientation of both conformations in the active site explains this discrepancy. The R enantiomers preferred to orient the benzylic carbon towards the phosphonate in a "backside-attack" like orientation (Figure 3.18), whereas the S enantiomers point their benzylic carbon away from the phosphonate in order to adopt the same ring orientation (Figure 3.19). In Figure 3.18, this conformation orients the R enantiomers' benzylic carbon well within 6 angstroms. However, the S enantiomers' conformation allowed their benzylic carbon to stray further from the phosphonate due to orientation. In addition, the chiral center of the S enantiomer positions the hydrogen towards the oxyanion hole loop as

opposed to the R enantiomers. This accounts for the increased measured distance between the ligands' ring structures and the alpha carbon of Gly-117.

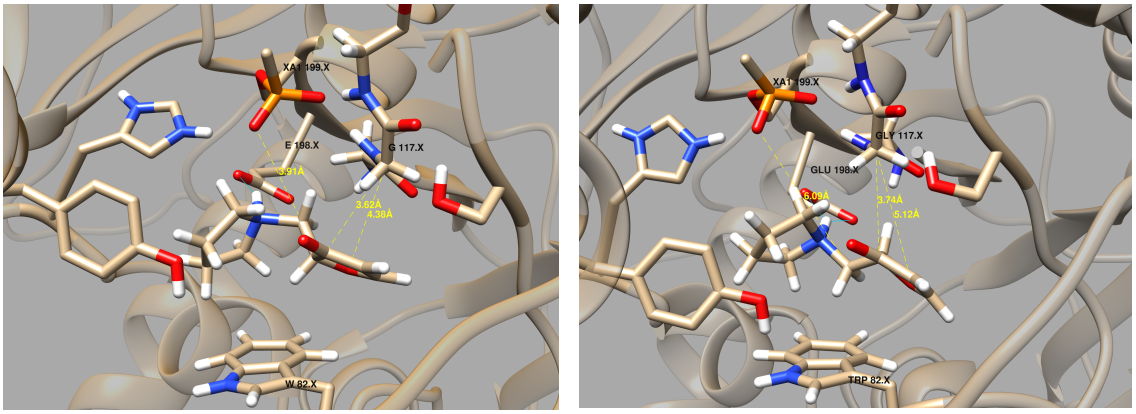

Figure 3.18 & 3.19: Representative poses of OH5R (left) and O5HS (right) in the active site during MD simulations.

Despite the R enantiomers being closer to the phosphonate, it is important to note that the analogous enantiomers are still adopting the same general conformations and interactions with the same relative frequency. The key advantage of the R enantiomers is that the benzylic carbon is orientated very well for a backside-attack realkylation. In this orientation, the benzylic carbon is very exposed to the phosphonate, regardless of the mechanism, possibly allowing for ease of realkylation. However, because the enantiomeric preference upon tautomerization is not controllable or predictable, the performance of both enantiomers needs to be considered.

As a whole, the keto-tautomers showed similar affinity for the active site as their enol counterpart but preferred distinctly different conformations. Due to the lack of an extra hydrogen bond donor, compounds prefer an orientation with VDW interactions with the omega loop and the oxyanion hole loop. While slightly further from aged serine residue, this orientation still positions the ligand within close distance where realkylation might be possible. However, these

compounds cannot act in a QMP elimination-type fashion, though this. Despite this, favorability of both tautomer forms has been demonstrated *in silico*, strengthening their potential as target realkylators.

4. Library 3 & 4: Neutral Variants

4.1 Introduction

Based on the success of Library 1 and Library 2 in addition to the pH in vitro screenings being performed, the neutral analogs of Library 1 and Library 2 were tested in the aged active site of AChE (Figure 4.1 & 4.2).

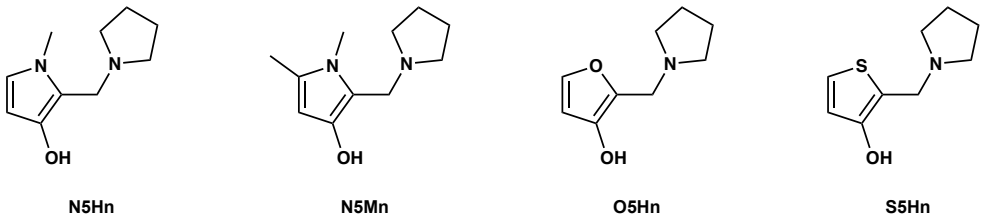

Figure 4.1: Library 3, the neutral analogs of Library 1.

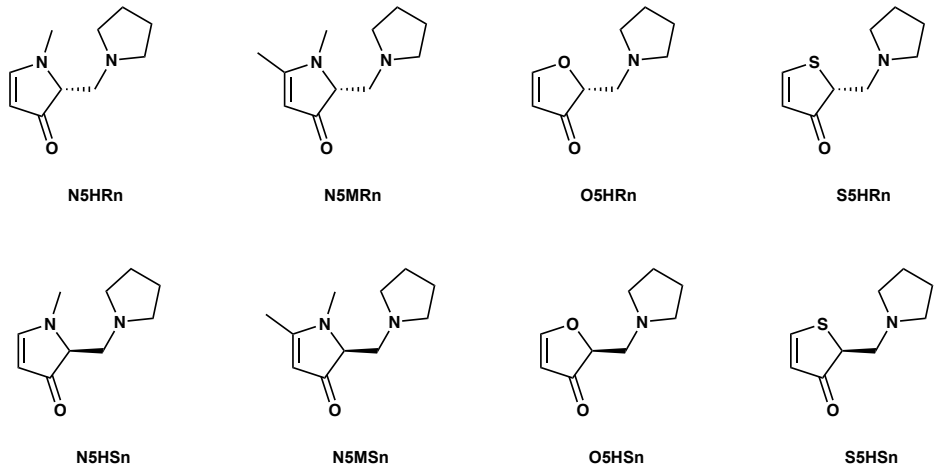

Figure 4.2: Library 4, the neutral analogs of Library 2.

As with enol tautomers, the keto forms were favored (Table 4.1), though by a smaller margin. This smaller margin can be attributed to the keto forms' lack of ability to hydrogen

bond. As such, the stabilization here is from the relief of steric strain or due to the electronic structure of the molecules themselves.

Table 4.1: The relative energy of the neutral tautomers.

Framework	Tautomer	Relative Energy (kcal/mol)
N5Hn	Enol	0
	Keto	-1.83
N5Mn	Enol	0
	Keto	-5.13
O5Hn	Enol	0
	Keto	-4.84
S5Hn	Enol	0
	Keto	-1.86

4.2 Molecular Docking Results

The neutral compounds consistently performed worse than the protonated compounds. Docking into more poses near in the bottleneck and less frequently under 4 Å (Figure 4.3-4.6, Table 4.2). This is consistent with what has been observed in other simulations. The neutral compounds lose a hydrogen bond donor on the amine group responsible for key interactions in the active site such as the phosphonate and Tyr-337. Additionally, the lack of a cation on these ligands limits interaction with the cation binding pocket, particularly with Trp-86 and Glu-202.

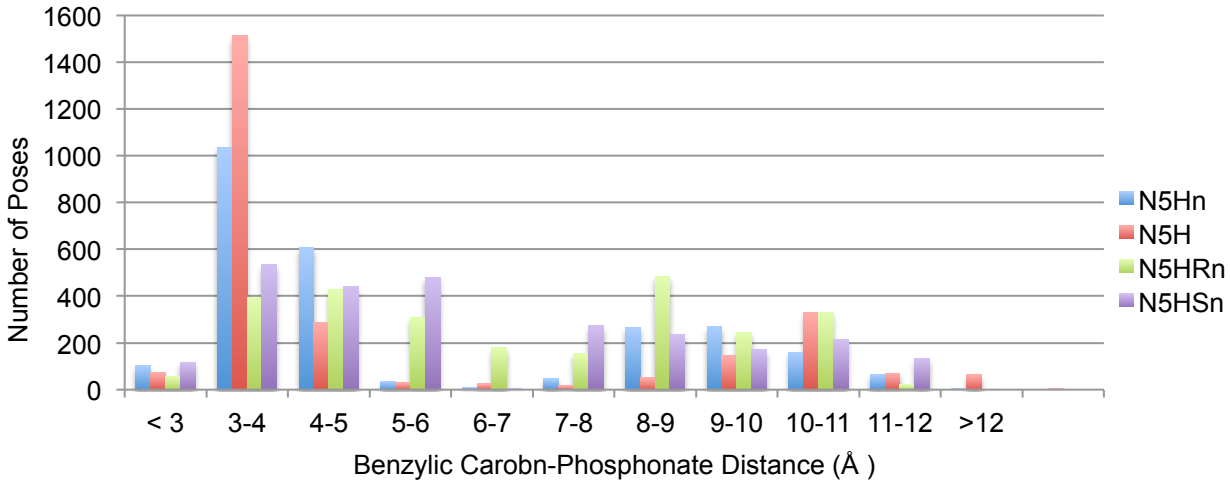

Figure 4.3: Benzylic carbon–phosphonate distance distribution of neutral N5H variants.

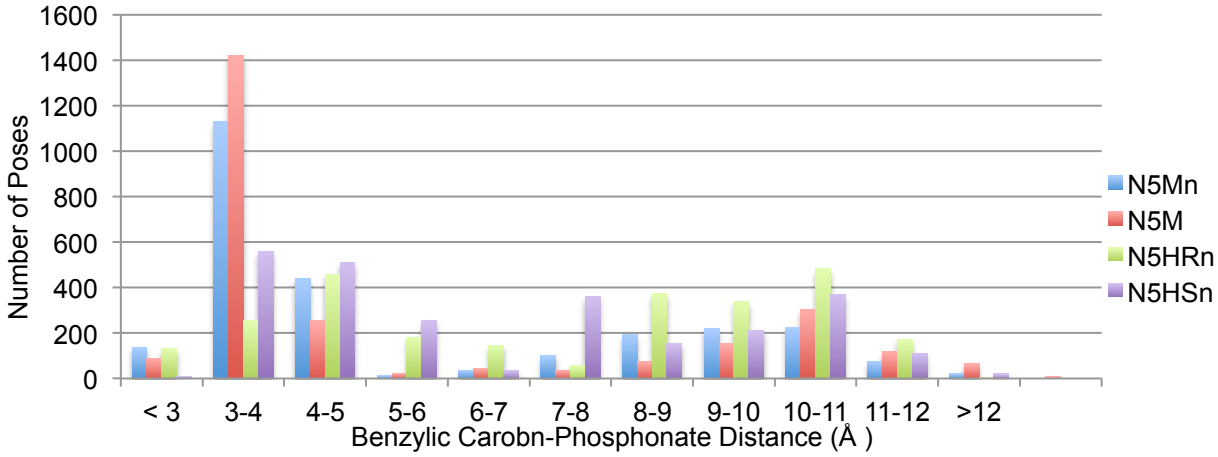

Figure 4.4: Benzylic carbon–phosphonate distance distribution of neutral N5M variants.

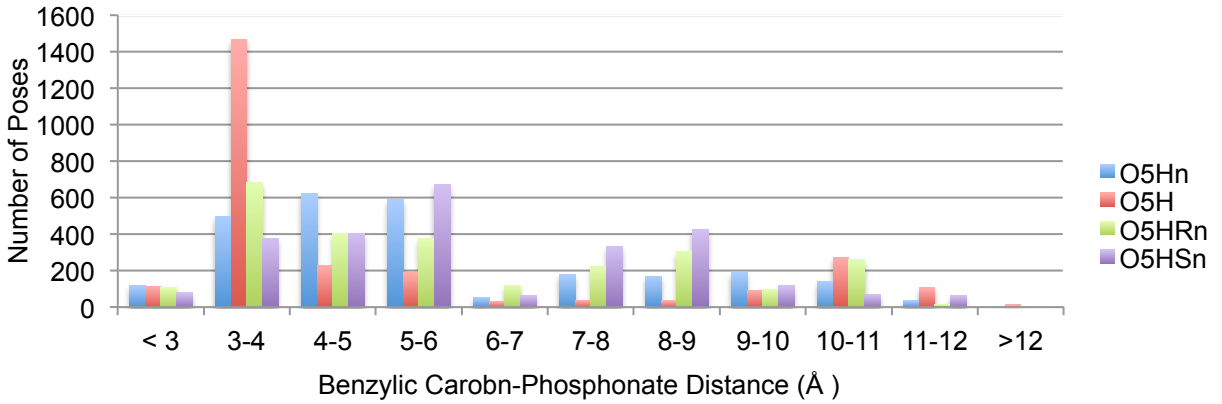

Figure 4.5: Benzylic carbon–phosphonate distance distribution of neutral O5H variants.

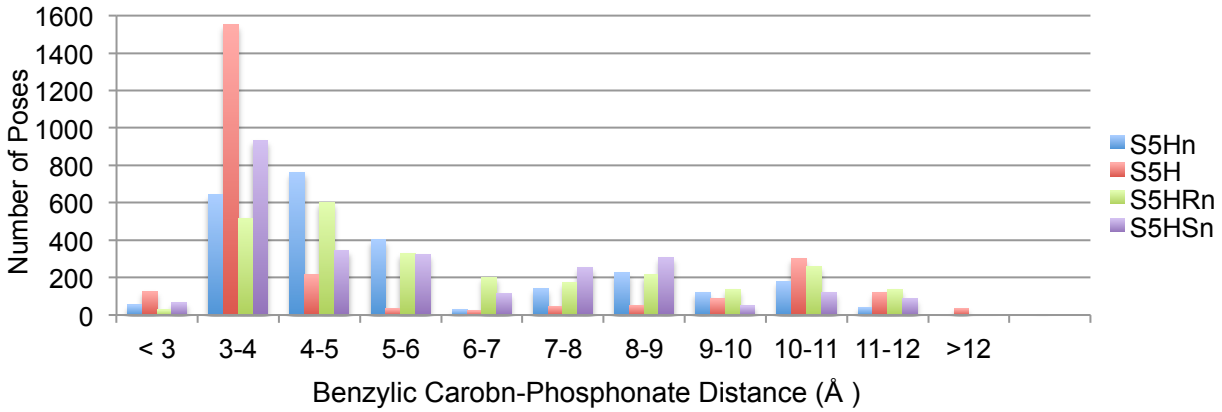

Figure 4.6: Benzylic carbon–phosphonate distance distribution of neutral N5H variants.

Table 4.2: Percent of poses ligands spends in each region of aged AChE

Ligand	% Active Site	% Between AS and BN	% Bottleneck	% Between BN and GM	% Gorge Mouth
N5Hn	67	2	19	4	9
N5Mn	66	2	15	5	13
O5Hn	48	25	18	3	7
S5Hn	56	17	15	3	9
N5HRn	34	19	27	7	14
N5HSn	42	19	21	5	13
N5MRn	32	13	23	6	25
N5MSn	42	11	21	6	19
O5HRn	46	19	22	3	11
O5HSn	33	28	31	3	5
S5HRn	44	20	17	3	15
S5HSn	52	17	22	1	8

When compared to eachother, the neutral enol compounds typically performed better than the neutral keto compounds, typically binding within 4 Å of the phosphonate more frequently (Table 4.2). The lack of any hydrogen bond donors can explain this. The discrepancy was most evident in the pyrrole compounds. In fact, the neutral enol pyrroles showed active site affinity similar that of their protonated counterparts and much higher than the neutral thiophene and furan compounds. The lowest energy conformations for each compound took on a similar conformation to Library 2, with the aromatic ring showing VDW interaction between the oxyanion hole loop and the omega loop (Figure 4.7). Unlike the keto-tautomers, the amine group cannot interact with Glu-202 and instead sit in front of Trp-86. This lowest energy conformation positions the benzylic carbon ~4 Å from the phosphonate, ideal for a backside-attack substitution.

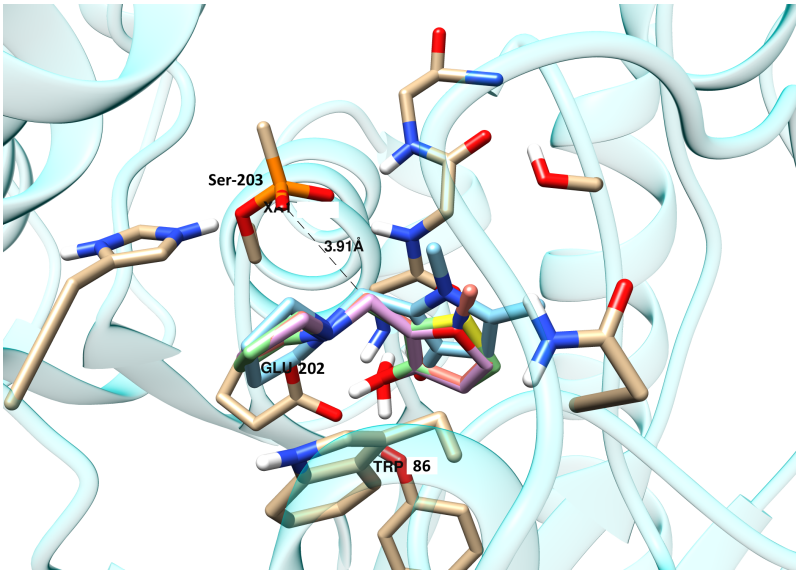

Figure 4.7: The lowest energy docked conformation of Library 3 in aged AChE. O5Hn (Pink), N5Hn (Red), N5Mn (Blue), S5Hn (Green).

4.3 Molecular Dynamics Results

The MD simulations verified that the ligands favored the bottleneck region of the AChE. Where the protonated compounds spent a majority of their time in the active site area, none of the Library 3 (neutral enol) compounds spend more than 40% of the time with a benzylic carbon –phosphonate distance less than 6 Å (Table 4.3) and only three of the Library 4 (neutral keto) compounds. While the hydroxyl group may have frequently acted as a hydrogen bond donor for the protonated compounds that may be more of a consequence of the ammonium group present on those compounds. The neutral ligands (without an ammonium group) saw little hydrogen bonding between the hydroxyl and the active site compared to their protonated counterparts (Table 4.4). Further, despite containing the hydroxyl group (the hydrogen bond donor), Library 3 performed similarly to Library 4. This suggests that the ligands that have demonstrated realkylation *in vitro* are likely in their protonated state or a zwitterionic state while in the active site and that the salt bridges and and cation-π interactions are the driving force behind ligand binding.

Table 4.3: Percent time benzylic carbon is within 4 Å of the phosphonate oxygen.

Ligand	% <4 Å	% <6 Å	% <8 Å	% >10 Å
N5Hn	8	37	76	12
N5Mn	12	39	74	17
O5Hn	13	34	61	16
S5Hn	10	31	71	13
N5HRn	6	33	68	11
N5HSn	4	31	78	6
N5MRn	1	26	56	18
N5MSn	3	29	72	6
O5HRn	11	40	77	9
O5HSn	5	45	69	10
S5HRn	5	38	75	11
S5HSn	8	48	77	8

Table 4.4: Percent of time hydroxyl group acts as a hydrogen bond donor to active site

Ligand	% H-bond to Glu-202	% H-bond to Phosphonate	% H-bond to Ser-125	%H-bond to Tyr-337
N5Hn	3	10	6	4
N5Mn	3	7	3	3
O5Hn	12	18	3	1
S5Hn	10	8	11	1

The absence of the ammonium group, a defining hydrogen bond donor and complimentary charge to the active site, saw many of these ligands remain in the bottleneck interacting largely with the omega loop with VDW type interactions (Table 4.5). Few polar interactions were observe in the MD simulations, so it was determined that the main force driving these compounds into the bottleneck were nonpolar VDW interactions. In order to give a rough assessment of this, the distance between the centroid between the alpha carbons of Asp-74 and Trp-86 with the centroid of the ring structures and the centroid of the pyrrolidine was measured (Figure 4.8 & Table 4.5). The neutral keto tautomers show the highest affinity for the omega loop, with their rings interacting 30-40% of the time. Their carbonyl group may be suited for the nonpolar environment near the bottleneck over the hydroxyl group on the neutral enols.

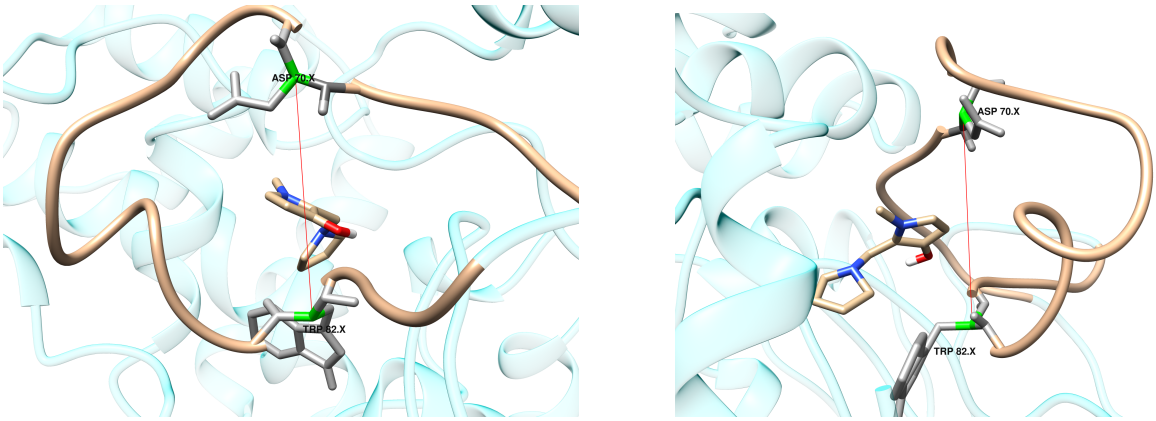

Figure 4.8 & 4.9: The centroid of the Asp-74 and Trp-86 alpha carbons

Table 4.5: Measurements of the ligands structures' interactions with omega loop

Ligand	% Ring Centroid (4 Å)	% Ring Centroid (5.5 Å)	% Pyrrolidine Centroid (4 Å)	% Pyrrolidine Centroid (5.5 Å)
N5Hn	19	27	11	19
N5Mn	15	22	10	15
O5Hn	9	13	20	28
S5Hn	19	25	17	29
N5HRn	24	33	5	19
N5HSn	23	34	7	16
N5MRn	22	38	5	22
N5MSn	23	42	7	25
O5HRn	18	30	9	20
O5HSn	11	25	3	7
S5HRn	28	36	8	23
S5HSn	18	28	14	19

As with the keto-tautomers, interaction with the oxyanion hole loop was measured as well as π-π interaction with Trp-86 (Table 2.6). However, without the presence of a cation, the active site often closed off during the MD simulations leaving little room for these interactions (Figure 4.10). The analysis shows that neither π-π with Trp-86 nor VWD with the oxyanion hole loop were favored. Compared to the keto tautomers, which typically spent more than 30- 40% of the time interacting with these residues, none of the neutral compounds exceeded 24% and most did not exceed 20%. These findings support that a positive cationic charge is necessary for the active site to open up an induced fit.

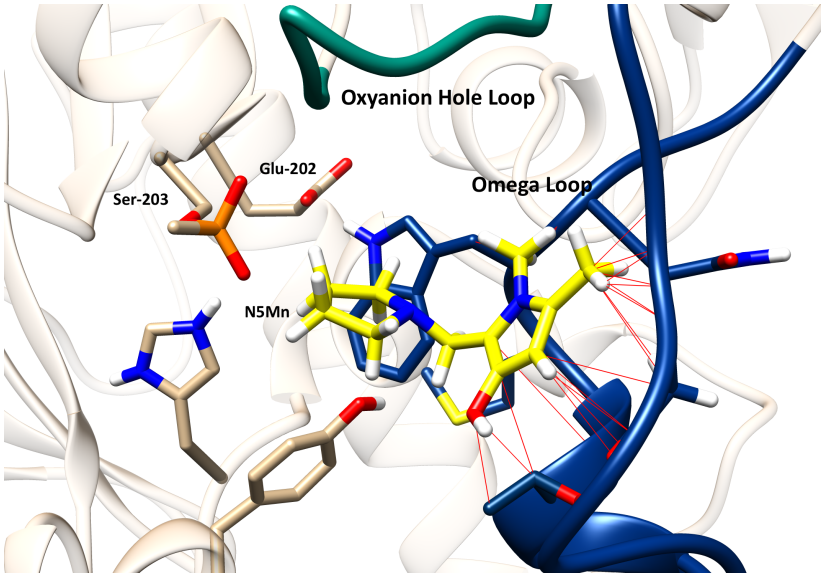

Figure 4.10: The omega loop and Trp-86 (navy) closed in on the active site, leaving the ligand (yellow) to form VDW interaction (red) with the omega loop.

Table 4.6: Aromatic and VDW interactions with the ring structures

Ligands	% Gly-121 Cα (4 Å)	% Gly-121 Cα (4.5 Å)	% π-π (4 Å)	% π-π (4.5 Å)
N5Hn	9	13	2	8
N5Mn	10	19	9	15
O5Hn	11	19	5	15
S5Hn	13	21	3	11
N5HRn	6	14	5	17
N5HSn	6	18	5	11
N5MRn	2	7	1	4
N5MSn	6	15	5	12
O5HRn	11	24	8	16
O5HSn	11	17	5	17
S5HRn	10	20	11	20
S5HSn	11	22	7	19

5. Library 5: Varied Leaving Group

5.1 Introduction

To this point, pyrrolidine has been used as the leaving group for each compound because of its *in silico* and *in vitro* success. However, previous studies, both computational[1] and experimental[2], have tested a variety of amine leaving groups to varied success. Diethyl amine has shown varying amounts of success computationally and experimentally as well as dimethyl amine and piperidine to lesser degrees. To see if these leaving group patterns are conserved with the smaller scaffold, Library 5 was tested (Figure 5.1).

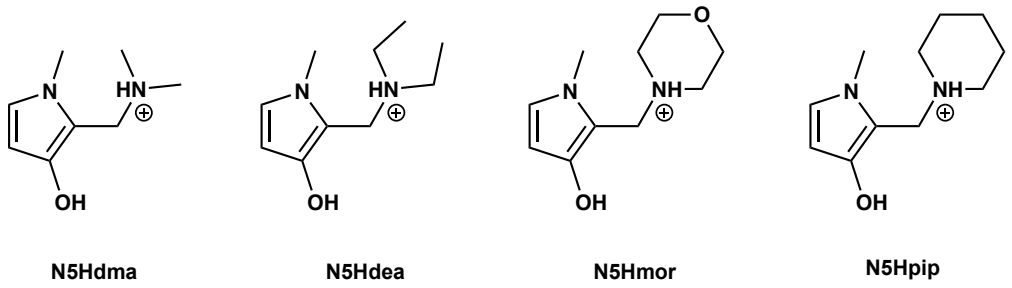

Figure 5.1: Library 5, N5H variants with different leaving groups.

5.2 Molecular Docking Results

The compounds in Library 5 all performed worse than N5H(pyr), all showing significantly less poses within the 3-4 Å range. This result is consistent with previous experimental and computational studies that routinely show pyrrolidine as the best performing leaving group. However, diethyl amine was posed near the phosphonate the least often, contrary to the experimental data.

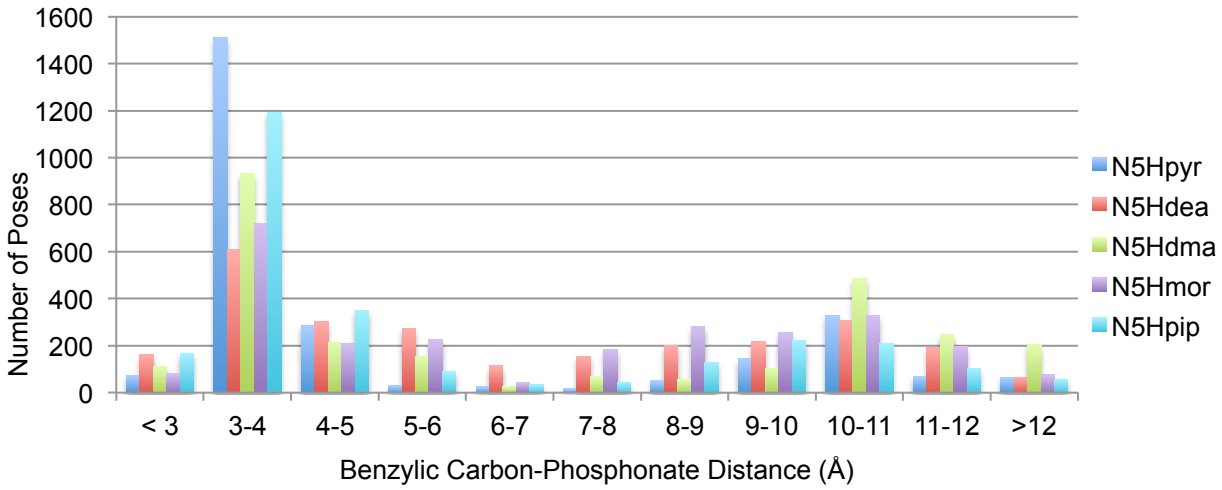

Figure 5.2: Benzylic carbon–phosphonate distance distribution for Library 5.

Analysis of the docking poses reveals that pyrrolidine and piperidine discourage cation-π interaction with Trp-86, due to their extra steric bulk (Figure 5.2). Subsequently, they are pushed closer to the phosphonate. This confirms what Blanton[1] found in his studies of leaving groups.

5.3 Molecular Dynamics Results

Table 5.1: Percent of time each ligand spends in cutoff ranges from the phosphonate

Ligand	% <4 Å	% <5 Å	% <6 Å
N5H(pyr)	56	61	76
N5Hdea	22	33	51
N5Hdma	20	30	48
N5Hmor	15	26	48
N5Hpip	18	25	46

The results from docking are exaggerated in the MD simulations, where N5H(pyr) spends significantly more time within 4 Å of the phosphonate as well as at each following cutoff (Table 5.1). However, one observation not conserved from docking is that piperidine did not perform well relative to the other compounds. It is possible that the extra bulk simply made binding near the active site more difficult when simulated over time. Aromatic interaction (Table 5.2) with Trp-86, though does qualify some of the heavy favorability of N5H(pyr). With the exception of N5Hdea, N5H showed the least affinity for cation-π interaction with Trp-86, so it is less drawn away from the posphonate and forms stable salt bridges with Glu-202 (Figure 5.4, 5.5).

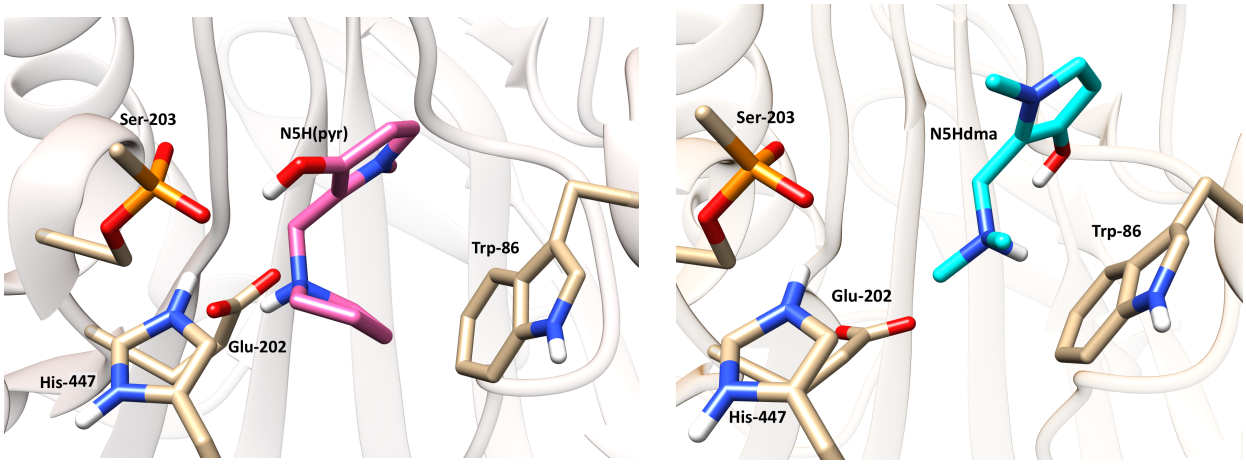

Figure 5.3 & 5.4: The pyrrolidine (left) sterically hindering cation-π and N5H (right) positioned near Trp-86.

Table 5.2: Percent of time each ligand interactions with Trp-86

Ligand	% Cation-π (4.5 Å)	% π-π (4.5 Å)
N5H(pyr)	11	15
N5Hdea	12	12
N5Hdma	21	24
N5Hmor	16	21
N5Hpip	17	18

Upon analysis of the MD simulations, N5Hdea was shown to hydrogen bond to the phosphonate anion, particularly with the ammonium group, much more than the other compounds with similar performance (Table 5.3). Frequently, the pose in Figure 5.5 was observed, where the ammonium hydrogen bonds to Glu-202. It is still unclear as to why this pose is favored primarily by this leaving group but does not show the all around favorability of N5H, but the flexibility offered by freely rotation N-substituents may be involved; allowing for enough steric hinderance to move closer to Glu-202, but not as much hindrance as pyrrolidine and failing to get much closer than ~5 Å.

Table 5.3: Percent of time each ligand hydrogen bonds to the phosphonate.

Ligand	% Ammonium-Phosphonate H-bond (3.5 Å)	% Hydroxy-Phosphonate H-bond (3.5 Å)
N5Hpyr	13	37
N5Hdea	30	22
N5Hdma	13	8
N5Hmor	15	22
N5Hpip	18	26

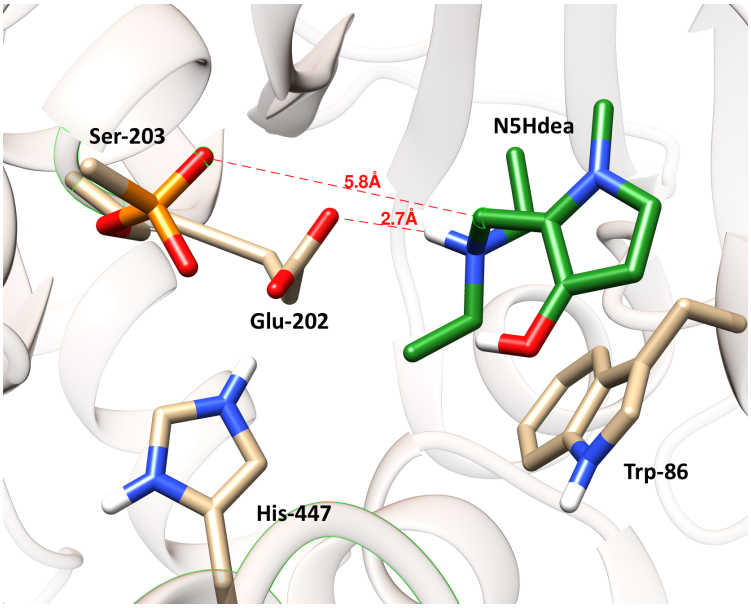

Figure 5.5: N5Hdea hydrogen bonding with Glu-202 across from phosphonate

However, the most important finding from this study is that pyrrolidine seems to be the most favorable amine leaving group of this set regardless of the scaffold. Confirming Blanton's conclusions[1], pyrrolidine strikes a good balance between being sterically hindered enough to push away from Trp-86 towards the phosphonate, but not too sterically hindered such that it is difficult to enter the active site. However, the affinity of the 5-member ring scaffold itself should not be overlooked, as it outperformed RD-o-5 with the same leaving group.

5.4 References

1. Blanton, T. G., Undergraduate Thesis, The Ohio State University, 2015.

2. Zhuang, Q.; Franjesevic, A.J.; Corrigan, T.S.; Coldren, W.H.; Dicken, R.; Sillart, S.; DeYong, A.; Yoshino, N.; Smith, J.; Fabry, S.; Fitzpatrick, K.; Blanton, T.; Joseph, J.; Yoder, R.J.; McElroy, C.A.; Ekici, O.D.; Callam, C.S., Hadad, C.M. "Demonstration of *in vitro* Resurrection of Aged Acetylcholinesterase after Exposure to Organophosphorus Chemical Nerve Agents" *Journal of Medicinal Chemistry*. **In Revision, submitted Feb. 2018.**

6. Conclusion and Future Work

6.1 Conclusions

This study evaluated the potential for substituted 5-member ring heterocycles as realkylators of aged AChE and gained a better understanding for the active site of aged-AChE. These compounds were shown to perform just as well or better than an *in vitro* and *in silico* lead compound in the same protonation state. Not only do these compounds spend equivalent or greater percent of time in the active site, but they have a higher affinity for orientations very close to the aged phosphonate anion due to a smaller π-π interaction with Trp-86. The stereochemistry for these compounds is also favorable, allowing both hydrogen bond donors to interact with anionic phosphonate and Glu-202.

Though, these compounds were shown to favor their keto tautomers, the keto tautomers also demonstrated an affinity for the active site. Frequently, the relatively hydrophobic ring without a hydroxyl group would be nestled in a pocket near phosphonate consisting of the omega loop and the oxyanion hole loop, allowing the ammonium to interact with Trp-86 and the anionic residues in the active site. The demonstrated affinity of both tautomers shows the potential of these compounds as realkylators. Though, the favored keto forms cannot react via a QM intermediate, an S_N2 style mechanism is certainly possible. In fact, if the keto compounds were shown experimentally to realkylate aged AChE, it would increase the certainty of the mechanism, suggesting a backside-attack.

The optimal amine for this framework was determined to be pyrrolidine. Consistently showing to be one of the best leaving groups, its benefit on these 5-member ring compounds was invaluable; it significantly increased active site affinity compared to the other leaving groups

tested. However, the success of these compounds should not be entirely attributed to the leaving group, as these compounds outperformed the lead framework with the same leaving group. Additionally, the analysis of the leaving group MD simulations agreed with previous findings, proving the consistency and reliability of the methods used.

The studies of the neutral compounds agree that these compounds (and others) have a high likelihood of entering the active site while protonated (or zwitterionic). The MD simulations showed that a lack of a cation on the ligand closed off the artificially enlarged active site. This ultimately results in the ligands remaining in the bottleneck near the omega loop.

Even though these compounds face uncertainty due to their instability and pose synthetic challenges, these 5-member ring heterocycles should be considered for experimental studies. Having demonstrated affinity for the active site at the same level or higher than known realkylators *in silico* (the greatest assurance that these computational methods can provide), these compounds will likely show similar affinity *in vitro*; their success or failure could also elucidate the realkylation mechanism. Additionally, these compounds are new and different to the many pyridinol and phenolic QMPs that have already been studied.

6.2 Future Work

Because we work in collaboration with experimentalists, a further step would naturally be to attempt synthesis for *in vitro* studies. However, if that proves to be too difficult other principles can be applied. As alluded to, zwitterionic derivatives are of great interest as they contain a cationic charge, but also a negatively charged oxygen. Because *in vitro* studies have had more success at higher pH, this may truly be the ideal state in which ligands enter the active site. Another direction would be to add methyl groups to already strong realkylators. The methyl group(s) on the pyrrole frameworks pushed the ligand closer to the phosphonate anion. Work has already successfully been done by adding methyl groups the leaving group, but adding to the pyridinol ring structure could prove beneficial.

In a different direction, computational effort could be put towards clarifying the mechanism of realkylation. This would need to be accomplished through QM/MM transition state calculations wherein certain parts of a large system can be treated with *ab initio* methods to accurately perform complex calculations while remaining resource efficient. This would be a new step for the project, as only the affinity for the active site has been studied, not actual realkylating potential.